

AD _____

Award Number: DAMD17-96-C-6086

TITLE: Thin Film CdZnTe Detector Arrays for Digital Mammography

PRINCIPAL INVESTIGATOR: Nader M. Kalkhoran

CONTRACTING ORGANIZATION: Spire Corporation
Bedford, Massachusetts 01730-2396

REPORT DATE: January 2001

TYPE OF REPORT: Final

PREPARED FOR: U.S. Army Medical Research and Materiel Command
Fort Detrick, Maryland 21702-5012

DISTRIBUTION STATEMENT: Approved for Public Release;
Distribution Unlimited

The views, opinions and/or findings contained in this report are those of the author(s) and should not be construed as an official Department of the Army position, policy or decision unless so designated by other documentation.

20010521 080

REPORT DOCUMENTATION PAGE

*Form Approved
OMB No. 074-0188*

Public reporting burden for this collection of information is estimated to average 1 hour per response, including the time for reviewing instructions, searching existing data sources, gathering and maintaining the data needed, and completing and reviewing this collection of information. Send comments regarding this burden estimate or any other aspect of this collection of information, including suggestions for reducing this burden to Washington Headquarters Services, Directorate for Information Operations and Reports, 1215 Jefferson Davis Highway, Suite 1204, Arlington, VA 22202-4302, and to the Office of Management and Budget, Paperwork Reduction Project (0704-0188), Washington, DC 20503

1. AGENCY USE ONLY (Leave blank)	2. REPORT DATE	3. REPORT TYPE AND DATES COVERED	
	January 2001	Final (26 Sep 96 - 25 Dec 00)	
4. TITLE AND SUBTITLE Thin Film CdZnTe Detectors for Digital Mammography			5. FUNDING NUMBERS DAMD17-96-C-6086
6. AUTHOR(S) Nader M. Kalkhoran			
7. PERFORMING ORGANIZATION NAME(S) AND ADDRESS(ES) Spire Corporation Bedford, Massachusetts 01730-2396 E-Mail: nkalkhoran@spirecorp.com			8. PERFORMING ORGANIZATION REPORT NUMBER
9. SPONSORING / MONITORING AGENCY NAME(S) AND ADDRESS(ES) U.S. Army Medical Research and Materiel Command Fort Detrick, Maryland 21702-5012			10. SPONSORING / MONITORING AGENCY REPORT NUMBER
11. SUPPLEMENTARY NOTES			
12a. DISTRIBUTION / AVAILABILITY STATEMENT Approved for Public Release; Distribution Unlimited			12b. DISTRIBUTION CODE
13. ABSTRACT (Maximum 200 Words)			
<p>The objective of this program was to develop large-area, flat-panel detectors for digital mammography using CdTe or CdZnTe deposited by metalorganic chemical vapor deposition (MOCVD) directly on thin-film transistor (TFT) active matrix arrays for image readout. CdTe and CdZnTe have the potential to meet the requirements for digital mammography due to their high x-ray absorption, large bandgap and good carrier transport.</p> <p>After four years of intensive work, we were able to deposit the key detector film on crystalline silicon multiplexors and TFT arrays, maintaining the integrity of underlying electronics in both cases and proving the possibility of the proposed technology. Unfortunately, CdZnTe thin films were never realized with electrical properties equal to bulk grown CdZnTe, and functioning detectors could not be obtained.</p>			
14. SUBJECT TERMS Mammography, CdTe, CdZnTe, array, MOCVD, TFT, hterojunction			15. NUMBER OF PAGES 65
			16. PRICE CODE
17. SECURITY CLASSIFICATION OF REPORT Unclassified	18. SECURITY CLASSIFICATION OF THIS PAGE Unclassified	19. SECURITY CLASSIFICATION OF ABSTRACT Unclassified	20. LIMITATION OF ABSTRACT Unlimited

FOREWORD

Opinions, interpretations, conclusions, and recommendations are those of the author and are not necessarily endorsed by the U.S. Army.

X Where copyrighted material is quoted, permission has been obtained to use such material.

X Where material from documents designated for limited distribution is quoted, permission has been obtained to use the material.

X Citations of commercial organizations and trade names in this report do not constitute an official Department of Army endorsement or approval of the products or services of these organizations.

N/A In conducting research using animals, the investigator(s) adhered to the "Guide for the Care and Use of Laboratory Animals," prepared by the Committee on Care and Use of Laboratory Animals of the Institute of Laboratory Resources, National Research Council (NIH Publication No. 86-23, Revised 1985).

N/A For the protection of human subjects, the investigator(s) adhered to policies of applicable Federal Law 45 CFR 46.

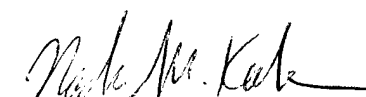
N/A In conducting research utilizing recombinant DNA technology, the investigator(s) adhered to current guidelines promulgated by the National Institute of Health.

N/A In the conduct of research utilizing recombinant DNA, the investigator(s) adhered to the NIH Guidelines for Research Involving Recombinant DNA Molecules.

N/A In the conduct of research involving hazardous organisms, the investigator(s) adhered to the CDC-NIH Guide for Biosafety in Microbiological and Biomedical Laboratories.



Prepared by: Anton C. Greenwald, Ph.D.
Senior Scientist



Nader M. Kalkhoran
Principal Investigator

TABLE OF CONTENTS

1	BODY of REPORT	2
1.1	Why is research important?.....	2
1.2	Summary Review of Program	5
1.3	Task 1 and Task 6 - Deposition of (Cd,Zn)Te	6
1.3.1	Evaporated Films.....	6
1.3.2	Chemical Vapor Deposition of CdTe and CdZnTe Thin Films	7
1.3.3	Low-Temperature Deposition	18
1.3.4	High-Temperature Deposition.....	18
1.4	Tasks 2, 3 and 4 - Passive Matrix Test Structure	19
1.5	Task 5 and 8 - Model (Cd,Zn)Te Detectors for Mammography, Prepare to characterize Silicon Multiplexors with (Cd, Zn)Te : work performed by Dr. Rowlands, subcontractor	23
1.5.1	Modeling of Absorption Efficiency	28
1.6	Tasks 7, 10 and 11	30
2	KEY RESEARCH ACCOMPLISHMENTS	32
3	REPORTABLE OUTCOMES	32
3.1	Publications.....	32
3.2	Presentations	32
4	CONCLUSIONS	34
5	REFERENCES.....	34

LIST OF FIGURES

Figure 1	Direct conversion flat panel concept.	3
Figure 2	Schematic diagram of the interdigitated pattern used for I-V measurements.....	7
Figure 3	I-V characteristics of CdTe layers grown by a) cold-wall evaporation method and b) hot-wall method.	7
Figure 4	Diagram of new MOCVD reaction chamber.	9
Figure 5	Diagram of gas supply system used for MOCVD of (Cd, Zn)Te.....	10
Figure 6	Surface morphology of CdTe grown by MOCVD on GaAs substrate, run #M4-4530 400 \times	11
Figure 7	Double crystal X-ray diffraction data for a thick (>50 μ m) CdTe layer on GaAs.	12
Figure 8	Infrared reflectance as a function of wavelength (nm) for CdTe layer grown by MOCVD on GaAs substrate. Sample #MO-4495-1.	12
Figure 9	Room-temperature transmission data for CdZnTe thin film deposited on glass substrates by MOCVD.	13
Figure 10	Growth rate for MOCVD-deposited CdTe as a function of temperature.	15
Figure 11	Profilometer plot of a CZT film (M4-4549) deposited on an ITO-coated glass substrate using a flat susceptor.	16
Figure 12	Profilometer plot of a CZT film (M4-4632) grown using a “pocketed” susceptor.	17
Figure 13	Resistivity as determined by current-voltage measurements for CdZnTe/ITO (open circles) and leakage current for CdZnTe/CdS/ITO (closed circles) versus growth rate at 250°C.	18
Figure 14	Illustration of CdTe/CdS heterojunction structure obtained from NREL.....	21
Figure 15	I-V characteristics of CdTe/CdS heterojunction structure obtained from NREL. The device shows improved leakage current performance over bulk thin-film material.	21
Figure 16	Schematic diagram of test setup used to evaluate CdTe/CdS heterojunction as a potential X-ray imaging detector.	22
Figure 17	Response of CdTe/CdS solar cell structure irradiated with alpha particles.....	22
Figure 18	Electron time of flight in an amorphous selenium sample.	24
Figure 19	Apparatus for the measurement of the time response of electroded samples and the response of an amorphous selenium sample to a 2 :s radiation pulse from a linac.	24
Figure 20	Measurement of pulse height spectra of photoconductor layers and examples of spectral broadening due to several physical effects (e) broadening due to trapping in the photoconductor layer $A_S \sim 0.9$, (f) broadening of the spectrum due to escape and partial re-absorption of K-fluorescent x-rays, $A_S \sim 0.7$	25

Figure 21	Schematic diagram of silicon multiplexer a) circuit diagram and b) plan view of top of multiplexer showing (black square) region where photoconductor is evaporated.....	27
Figure 22	Modular readout system for flat panel imager described in text.....	27
Figure 23	X-ray spectrum from a tungsten tube at 50 kV constant potential at the tube output (solid) and after attenuation by 5 cm of soft tissue (dotted).....	28
Figure 24	Absorption efficiency for x-ray spectra shown in Figure 23 as a function of film thickness for CdTe and Se.....	29

LIST OF TABLES

Table 1	The properties of photoconductors proposed for use in mammography.	4
Table 2	Summary of sheet resistance data for thermally evaporated CdTe thin film.....	8
Table 3	Sheet resistance data of CdZnTe layers deposited by thermal evaporation methods. The resulting resistivity is similar to that obtained for CdTe layers.	9
Table 4	Sheet resistance data of CdZnTe layers deposited by MOCVD.....	13
Table 5	Summary of a series of CdTe MOCVD runs conducted at 500 torr pressure, VI/II=2.9, using dimethylcadmium (DMCd) and dimethyltellurium (DMTe). All films were deposited on semi-insulating GaAs substrates (2° off 100 orientation).....	14
Table 6	Properties of selected tellurium precursors (Ref.).	15
Table 7	Summary of MOCVD experiments aimed at studying Zn incorporation. Zn concentration was determined from optical transmission measurements.	17
Table 8	MOCVD Growth Parameters and Film Characteristics.....	20

INTRODUCTION

The most promising approach for improving diagnostic accuracy in x-ray mammography is replacement of film-based systems with digital x-ray imaging systems. Available digital x-ray imaging systems employ amorphous silicon (a-Si) thin-film transistor (TFT) arrays in conjunction with phosphor screens or scintillator crystals that absorb x-rays and emit visible or near-IR light. A photodiode integrated with each TFT converts the light into an electrical signal. A more efficient system that would allow reduced x-ray dose would replace this two-step conversion process by a direct-conversion method, in which a photoconductor absorbs X-rays and generates an electrical signal directly. Several direct-conversion materials have been discussed, including amorphous selenium (a-Se),¹ lead iodide (PbI_2),² mercuric iodide (HgI_2)³ and thallium bromide ($TlBr$).⁴ Reasonable success has been achieved with each of these materials, but none has the combination of high resistivity and good carrier transport properties required for optimum detection efficiency. We proposed to demonstrate a digital imaging mammography system using cadmium zinc telluride ($CdZnTe$), a material with superior bulk properties, deposited on TFT arrays by metalorganic chemical vapor deposition (MOCVD). After four years of intensive work we were able to deposit the key detector film on crystalline silicon multiplexors and TFT arrays, maintaining the integrity of underlying electronics in both cases and proving the possibility of the proposed technology. Unfortunately, $CdZnTe$ thin films were never realized with electrical properties equal to bulk grown $CdZnTe$, and functioning detectors could not be obtained.

1 BODY OF REPORT

1.1 Why is research important?

The objective of this four-year program was to develop a large-area, flat-panel solid-state X-ray detector for digital mammography using thin-film CdTe or CdZnTe deposited directly on a thin-film transistor (TFT) active matrix array for image readout. If successful, this technology held the promise of improving early detection of tumors in the breast.

There has recently been a great deal of interest in digital radiology.⁵ Unlike other medical imaging modalities such as CT, ultrasound, or MRI, x-ray imaging remains largely an analog technique. The advantages of digital radiology are:

- co-registration and comparison of x-ray images with images acquired from other digital modalities;
- decoupling of image acquisition and display;
- simplified storage and instantaneous access without requiring locating and transporting film to each viewer;
- resilience to damage, and prolonged lifetime and lower loss risk;
- the possibility of teleradiography where remote locations could be serviced by highly trained personnel at a central hospital or health science center.

Currently there are two digital x-ray imaging techniques in widespread use. In the first technique a latent image stored in a stimulable phosphor is digitized by scanning with a laser. In the second technique the signal from a camera coupled to an x-ray image intensifier is digitized. Although the x-ray image intensifier can work at fluoroscopic imaging rates it has several disadvantages:

- the input phosphor is curved leading to pincushion distortion;
- veiling glare from scattered x-rays and internal reflection of light;
- poor resolution due to the coupling of several image conversion stages;
- susceptibility to magnetic fields leading to S-distortion,
- the intensifier itself is bulky reducing the free movement of the detector, limiting the viewing angles available.

A large area, flat-panel digital x-ray imaging detector has been shown to be a significant improvement over current radiological imaging methods.⁶ The basic concept of an active matrix readout system for a photoconductor detector is shown in Figure 1. The active matrix consists of an array of TFTs connected to pixel electrodes and storage capacitors. The TFTs are turned on row by row, and the signal is sent out through the source of the TFTs through separate signal lines. In order to make the active matrix sensitive to x rays, a photoconductor layer is evaporated onto the panel and a field is applied by connecting the top electrode to a potential. X-rays are absorbed in the photoconductor releasing electrons and holes that drifts towards their respective electrodes under the influence of the applied field, E_{ph} . Once the charge reaches the pixel electrodes it is stored and read out by the active matrix as discussed above.

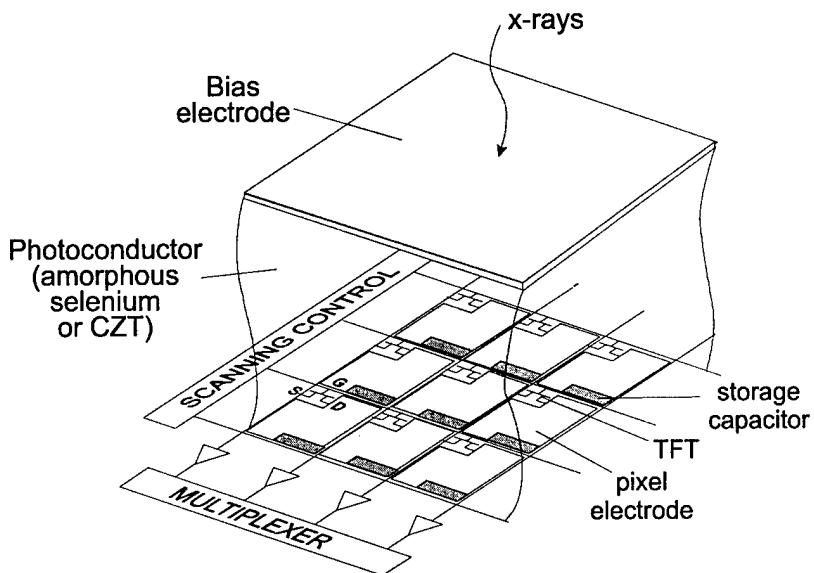


Figure 1 Direct conversion flat panel concept.

In order to have good image quality, the photoconductor must have several important properties. It must have large band gap energy, to limit the thermal generation of charge carriers in the bulk. This limits the use of photoconductors for x-ray imaging to those that have a band gap greater than 2 eV. Amorphous selenium, (*a*-Se), Lead iodide, (PbI_2), and cadmium zinc telluride, (CZT), are possible candidates. The photoconductor should have good bulk charge transport properties, to allow the charge image to reach the pixel electrodes before the charges are lost in traps, and it should have poor surface conductivity to prevent the lateral conduction of the image charge once it has reached the pixels. The photoconductor should be stable under the conditions of use, and over the lifetime of the imaging system. A final important property is a high x-ray to charge conversion efficiency. Recent measurements have shown that the conversion energy of amorphous selenium is 42 eV/e-hp at an applied field of $10\text{ V}/\mu\text{m}$. The conversion energy of PbI_2 and CZT is $\sim 5\text{ eV}/\text{e-hp}$.^{7,8} An interesting question that arises is whether 42 eV/e-hp is enough to work well in mammography or if 5 eV/e-hp is required. The answer to this question depends on whether simple radiography is required (in which case the gain of amorphous selenium is adequate). However, for more complicated imaging sequences for mammography made feasible by digital radiography (*e.g.* digital tomosynthesis, dual energy imaging and digital subtraction angiography) require many more images to be acquired at lower x-ray exposure and this requires the increased gain of the more advanced photoconductors to overcome noise from the active matrix panel.⁹ The advantage of amorphous selenium are that it has already been developed to the point that the desired charge transport properties in the bulk and on the surface have been achieved, it is stable (with the addition of $\sim 1\%$ As, and ppm Cl), and it can be made to any desired size due to the simplicity and scalability of the evaporation process used, and it is compatible chemically and thermally with active matrix substrates due to its low processing temperature which is due to the need to maintain the amorphous *i.e.* low temperature state of the material. Thus to gain the advantage of a decreased conversion energy compared to *amorphous selenium* the other desirable properties of a photoconductor have to be established in these novel photoconductors. What then are the properties of the competing materials, and how do they compare with amorphous selenium? In Table 1 we have listed the current capabilities of all three materials.

Table 1 The properties of photoconductors proposed for use in mammography.

Material	Conversion Efficiency	Resistivity ($\Omega\text{-cm}$)	Field (V/ μm)	Density (g/cm^3)	Dark Current
CZT	5 eV/ehp	$1.8\text{-}3.3 \times 10^{10}$	0.1	5.7	$1 \times 10^{-7} \text{ A cm}^{-2}$
PbI ₂	5 eV/ehp	5×10^{12}	1.0	6.16	$2 \times 10^{-9} \text{ A cm}^{-2}$
A-Se	42 eV/ehp	10^{15}	10	4.26	$1 \times 10^{-10} \text{ A cm}^{-2}$

In contrast, for the materials PbI₂ and CZT, which have usually been made in the form of single or polycrystals the situation, is not so well developed. Single crystal PbI₂ has been used in spectrometers, and deposited PbI₂ has been used in a 1" vidicon for x-ray imaging in real time,² and has shown good modulation transfer function, (MTF). Thicknesses of 150 - 250 μm have been reported.² Cadmium zinc telluride is a large band gap photoconductor that has been used in prototype medical imaging devices such as gamma cameras for SPECT imaging.¹⁰ It has also been used in small area linear imaging systems and has been shown to operate in real time.¹¹ CZT is similar to PbI₂ in that it has excellent quantum efficiency and there is difficulty in making high quality layers covering a clinically relevant area. It is also necessary in CZT to address the problems of low charge collection efficiency due to the low mobility-lifetime product of the holes combined with the low fields typically used in CZT because of high dark current.^{12,13} Thus work to improve the dark current is desirable.

It is important when designing a new x-ray imaging system first to establish the requirements of the imaging task and then ask to what extent the proposed new imaging system can meet them rather than the other way around. For mammography, there is the need to be able to see very small objects (micro calcifications) as well as subtle tissue density changes. These features must be visible to the radiologist and be obtainable with the normal x-ray exposure or preferably less. Our systematic evaluation of the required spectra indicated that it is necessary to use very low beam energy whatever the nature of the detector is.^{14,15} However, there is a balance between the optimum thickness due to factors related to resolution and quantum efficiency. We have extended the work already performed for amorphous selenium detectors to include CZT. Calculations indicate that the absorption of CZT is practically identical to amorphous selenium for the same thickness of material. However, there is an improvement in the Swank factor (derived from the scintillation spectrum) by using CZT rather than amorphous selenium as the mean energy of the optimum x-ray spectrum is close to the K-edge of amorphous selenium but is not exceeded for CZT. There will also be differences due to the higher gain of CZT.¹⁶

High efficiency, direct detection of x-rays with a very high x-ray-to-electron gain is an attractive feature of CZT detector technology. This is essential to ensure high image quality combined with the ability to make the layer in large areas. Our plan was to investigate CZT thin film layers production by the MOCVD process and test this material for its x-ray and imaging properties.

1.2 Summary Review of Program

We had planned to develop this detector array in three phases. The first phase was to develop the necessary CdTe or CdZnTe thin films. As part of the effort, we would design and fabricate CdTe or CdZnTe passive matrix detector test arrays with pixel sizes varying from 50 μm to 500 μm on various substrates including glass, gallium arsenide (GaAs), and silicon (Si). Passive matrix detector arrays are relatively simple to fabricate and do not require extensive electronics for testing. These arrays would allow us to measure detection efficiency, signal linearity, pixel size effects, optimum operating voltage, leakage current, and pixel-to-pixel uniformity. The results of these experiments would be used to optimize deposition conditions and detector design parameters. Spire would deposit the films and would design and fabricate the passive matrix detector arrays. Professor John Rowlands from the University of Toronto would characterize the arrays and perform theoretical calculations to determine parameters such as signal level, detection efficiency, X-ray quantum noise, and inherent spatial resolution.

In the second phase we had proposed to integrate prototype CdTe or CdZnTe detector arrays with Si multiplexers. Optimized deposition conditions for the CdZnTe films determined in the first stage were to be employed. A Si multiplexer was selected because of its lower cost than the CdSe TFT arrays ultimately to be used. We had planned to employ a 128 x 128 matrix array with 60 μm center-to-center element spacing. Spire was to deposit the thin films on the Si multiplexers, and the University of Toronto was to test these arrays.

In phase three, once the detector fabrication process and the electronics are determined, we had planned to develop a 5 cm x 5 cm prototype self-scanned detector array by integrating thin-film CdTe or CdZnTe detectors with a CdSe TFT array. The purpose of developing a 5 cm x 5 cm prototype was twofold: first, these arrays would be useful for stereotaxic breast biopsy, and second, they would be a first stage demonstration of an 18 x 24 cm large-area detector suitable for digital mammography. The prototype was to be developed jointly with Professor Rowlands and Litton Systems Canada, Ltd., the only North American vendor of CdSe TFTs, and was planned to have 1024 x 1024 50- μm pixel elements. Spire would deposit the CdZnTe detectors on these TFT arrays. Professor Rowlands, in collaboration with Spire, would assemble and characterize the detector arrays. Finally, phantom images using these arrays were to be obtained to demonstrate the usefulness of this approach for digital mammography.

The original statement of work for this program contained fifteen tasks listed below. At the conclusion of the program, tasks 1 and 5 were completed, work had begun on tasks 2, 3, 4, 6, 7, 8, 10, and 11. No work was attempted for tasks 9, 12, 13, 14 and 15. Material characteristics, low resistance, prevented testing x-ray detectors. (See conclusions, section 4).

- Task 1 Deposit and Characterize CdZnTe Thin Films on Glass and Si Substrates
- Task 2 Design of Passive Matrix Test Structure
- Task 3 Fabrication and Characterization of Passive Matrix Test Structure
- Task 4 Testing of Passive Matrix Detector Test Structure
- Task 5 Model CdZnTe Detectors for Digital mammography
- Task 6 Optimization of CdZnTe Deposition Conditions
- Task 7 Deposition of CdZnTe Thin Films on Si Multiplexors
- Task 8 Characterize CdZnTe Tin Films on Si Multiplexors
- Task 9 Optimize CdZnTe Detector Structure on Si Multiplexors

- Task 10 Deposition of CdZnTe Thin Films on CdSe Thin Film transistors
- Task 11 Characterization of CdZnTe Thin Films on CdSe Thin Film transistors
- Task 12 Design a Prototype 5 cm by 5 cm CdZnTe Detector with CdSe TFTs
- Task 13 Characterization and Testing CdZnTe Detectors on CdSe TFTs
- Task 14 Optimization of CdZnTe-CdSe TFT Processing
- Task 15 Demonstration of 5cm by 5cm CdZnTe Detector array for Digital Mammography

1.3 Task 1 and Task 6 - Deposition of (Cd,Zn)Te

The primary objective of this task was to deposit thin films of (Cd,Zn)Te suitable for X-ray detection. Both CdTe and CdZnTe thin film materials were deposited using metalorganic chemical-vapor deposition (MOCVD) and thermal evaporation techniques. A variety of substrates were used including indium tin oxide (ITO) coated glass, GaAs, and silicon. Growth conditions such as temperature, pressure, VI-II gas ratio, were varied. Resulting films were characterized for surface morphology, crystal quality, thickness, electrical properties, and zinc content for the CdZnTe samples. CdTe layers on GaAs substrates had excellent crystalline structure with deposition rates as high as 25 $\mu\text{m}/\text{hour}$. CdTe layers with thickness in the range of 20 to 50 μm were deposited on ITO coated glass substrates and tested for electrical properties.

1.3.1 Evaporated Films

One of the main objectives of this program is to develop a relatively low-cost deposition process for CdZnTe films. As a first step toward achieving this goal, we considered CdTe films grown by thermal evaporation using both cold-wall and hot-wall methods. We fabricated samples on glass substrates using the cold-wall method at growth temperatures ranging from room temperature to 100 °C. Lockheed Martin Infrared Imaging Systems (LMIRIS) provided samples grown by the hot-wall method on sapphire substrates. In both cases, the measured film thickness was roughly 2000 Å.

Sheet resistance measurements were taken for samples produced by both evaporation methods. The interdigitated pattern shown in Figure 2 was produced using photolithography. The metal contact layers were Au/Cr to provide good adhesion as well as ohmic contact to the CdTe thin film. An HP4145B semiconductor parameter analyzer was used to carry out I-V measurements over a ± 100 volt range, and the resulting data are illustrated in Figure 3. The sheet resistance of the CdTe surface was then determined using the relation:

$$R_{\square} = (V / I) \times (w / l)$$

where R_{\square} is the sheet resistance in ohms / square, V and I are taken from a point given in the Figure 3 data, and w and l are the respective width and length of the regions separating the interdigitated fingers. For films deposited by both methods, we measured sheet resistance at 100 volts to be approximately 10^{11} ohms / square. A summary of the CdTe film properties is provided in Table 2. These results show that the CdTe layers deposited by the cold-wall evaporation method have an order of magnitude lower sheet resistance (10^{11} ohms / square) compared to the CdTe layers deposited by the hot-wall evaporation method (10^{12} ohms / square). These results suggest a bulk resistivity value on the order of 2×10^7 ohm-cm which is not sufficient to achieve the low leakage current required for high performance detector operation. To increase the resistivity, we considered CdZnTe films since the bulk resistivity of CdZnTe alloys is known to be three orders of magnitude higher (10^{10} ohm-cm) than that of CdTe.

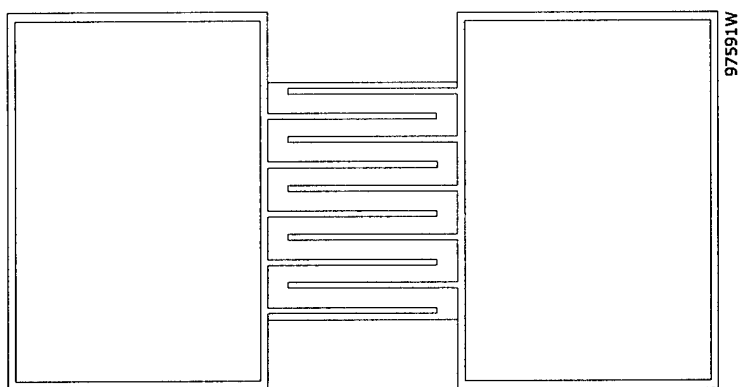


Figure 2 Schematic diagram of the interdigitated pattern used for I-V measurements. Au/Cr layers were chosen in order to make good ohmic contact to the CdTe thin film.

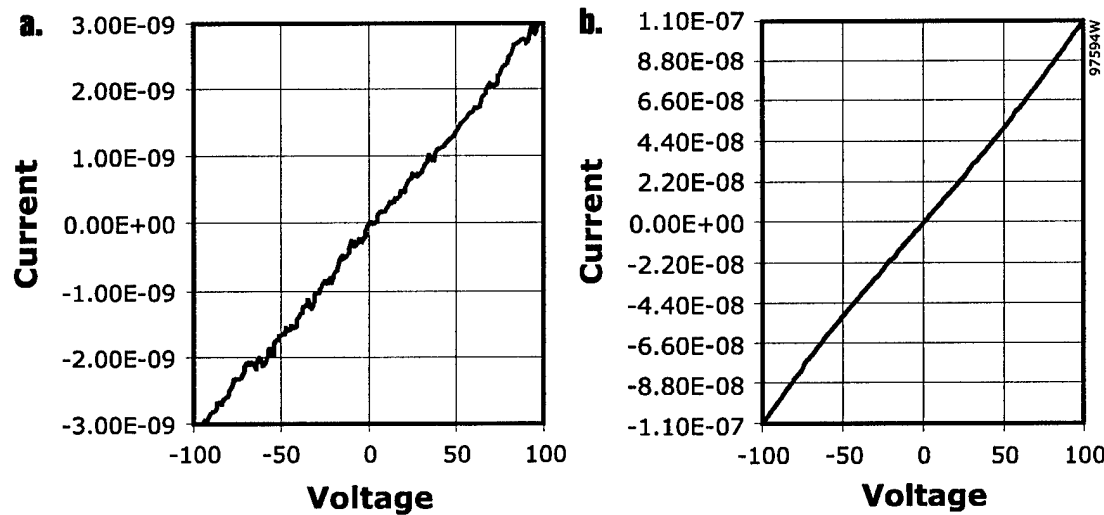


Figure 3 I-V characteristics of CdTe layers grown by a) cold-wall evaporation method and b) hot-wall method.

High pressure Bridgman (HPB) CdZnTe bulk samples as a source material for evaporation. The Zn composition in the HPB CdZnTe was 10% and the bulk resistivity of these samples was 5×10^{10} ohm-cm. During deposition, the substrate was held at room temperature. The sheet resistivity of these films were measured as described earlier, and Table 3 shows the sheet resistivity data. Unexpectedly, the sheet resistance of the resulting CdZnTe layers is still in the 10^{12} ohm /square range.

1.3.2 Chemical Vapor Deposition of CdTe and CdZnTe Thin Films

The process used to deposit superior (Cd,Zn)Te films during most of this program is commonly described as metalorganic chemical vapor deposition, or MOCVD. The reaction vessel used to deposit films is shown schematically in Figure 4, and the gas feed system is shown diagrammatically in Figure 5.

Table 2 Summary of sheet resistance data for thermally evaporated CdTe thin film.

SAMPLE ID	Deposition Temp. (°C)	Thickness (Å)	V (volts)	I (amps)	R (ohms)	R _n (ohms /sq)
E50091A	50	2235	-100	-1.65E-07	6.06E+08	2.08E+11
E50091B	50	2235	-100	-1.10E-07	9.09E+08	3.13E+11
E50091C	50	2235	-100	-1.21E-07	8.26E+08	2.84E+11
E50091A	50	2235	-100	-4.30E-08	2.33E+09	2.12E+11
E50091B	50	2235	-100	-2.65E-08	3.77E+09	3.43E+11
E50091C	50	2235	-100	-3.42E-08	2.92E+09	2.66E+11
E50092A	100	2335	-100	-2.60E-08	3.85E+08	1.32E+11
E50092B	100	2335	-100	-2.33E-08	4.29E+08	1.48E+11
E50092C	100	2335	-100	-1.84E-08	5.43E+08	1.87E+11
E50092A	100	2335	-100	-6.51E-08	1.54E+09	1.40E+11
E50092B	100	2335	-100	-5.98E-08	1.67E+09	1.52E+11
E50092C	100	2335	-100	-4.61E-08	2.17E+09	1.97E+11
E50093A	RT	2400	-100	-1.09E-07	9.17E+08	3.16E+11
E50093B	RT	2400	-100	-1.09E-07	9.17E+08	3.16E+11
E50093C	RT	2400	-100	-9.81E-08	1.02E+09	3.51E+11
E50093A	RT	2400	-100	-2.85E-08	3.51E+09	3.19E+11
E50093B	RT	2400	-100	-2.74E-08	3.65E+09	3.32E+11
E50093C	RT	2400	-100	-2.45E-08	4.08E+09	3.71E+11
E50094A	50	1206	-100	-7.76E-08	1.29E+09	4.43E+11
E50094B	50	1206	-100	-8.81E-08	1.14E+09	3.90E+11
E50094C	50	1206	-100	-9.25E-08	1.08E+09	3.72E+11
E50094A	50	1206	-100	-1.90E-08	5.26E+09	4.79E+11
E50094B	50	1206	-100	-2.07E-08	4.83E+09	4.40E+11
E50094C	50	1206	-100	-2.31E-08	4.33E+09	3.94E+11

HOT WALL EVAPORATION

LM-1A	RT	-	-100	-1.16E-08	8.62E+09	2.97E+12
LM-1B	RT	-	-100	-1.16E-08	8.62E+09	2.97E+12
LM-1A	RT	-	-100	-2.61E-09	3.83E+10	3.49E+12
LM-1B	RT	-	-100	-2.79E-09	3.58E+10	3.26E+12
LM-2A	RT	-	-100	-1.34E-08	7.46E+09	2.57E+12
LM-2B	RT	-	-100	-1.94E-08	5.15E+09	1.77E+12
LM-2A	RT	-	-100	-3.18E-09	3.14E+10	2.86E+12
LM-2B	RT	-	-100	-3.49E-09	2.87E+10	2.61E+12

Table 3 Sheet resistance data of CdZnTe layers deposited by thermal evaporation methods. The resulting resistivity is similar to that obtained for CdTe layers.

Sample ID	Material	Thickness (Å)	Voltage (Volts)	Current (Amps)	R (ohms)	R_{\square} (ohms /sq)
E50106A	CdZnTe	2000	-100	-3.60E-08	2.78E+09	9.56E+11
E50106B	CdZnTe	2000	-100	-3.15E-08	3.17E+09	1.09E+12
E50106C	CdZnTe	2000	-100	-3.57E-08	2.80E+09	9.64E+11
E50106A	CdZnTe	2000	-100	-1.05E-08	9.52E+09	8.67E+11
E50106B	CdZnTe	2000	-100	-8.72E-09	1.15E+10	1.04E+12
E50106C	CdZnTe	2000	-100	-8.95E-09	1.12E+10	1.02E+12

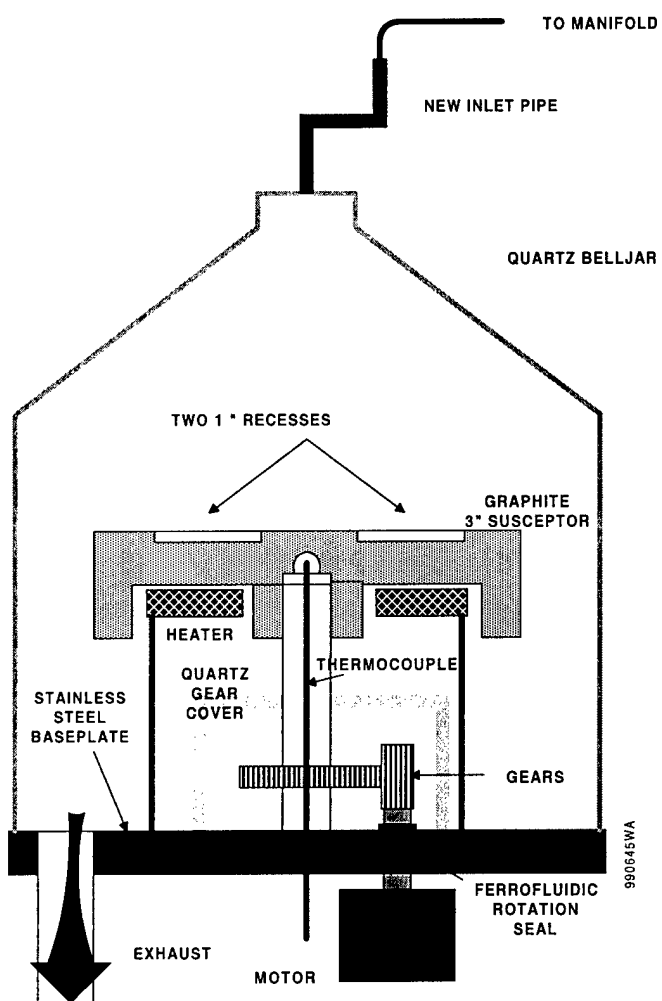


Figure 4 Diagram of new MOCVD reaction chamber.

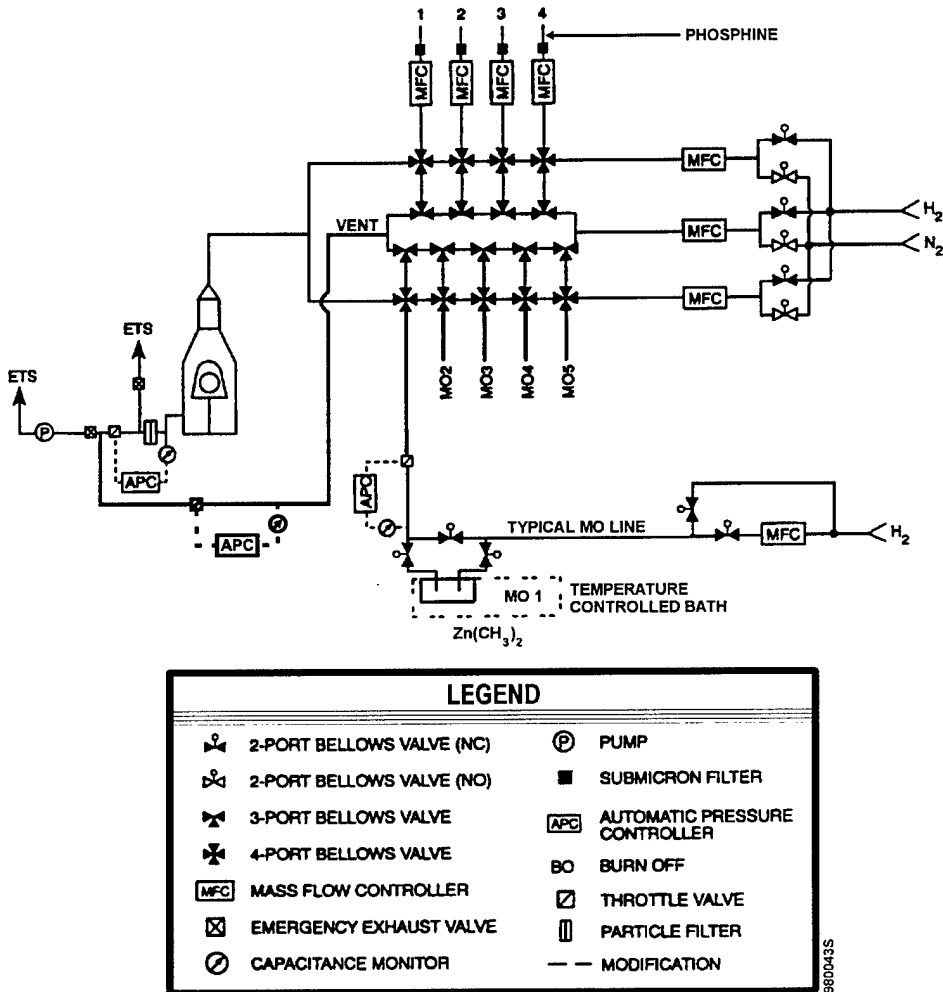


Figure 5 Diagram of gas supply system used for MOCVD of (Cd, Zn)Te

A short description of the process follows so the reader, assumed to be more familiar with radiation detectors as opposed to MOCVD, can understand the description of experiments. A gas mixture, mostly inert components, is fed into the reaction vessel at the top and flows over the heated substrates. Metallic compounds are adsorbed onto the surface and react there to form non-volatile (Cd, Zn)Te. Organic species combine to form volatile compounds that desorb from the surface. Resulting material is of higher purity than evaporated films (unless the latter is performed under ultra-high vacuum, such as MBE). Film qualities depend upon the reaction chamber pressure, total gas flow rate and temperature of the substrate.

The organo-metallic source compounds are liquid at room temperature and have a high vapor pressure. These are kept in a sealed "bubbler" maintained at a measured pressure. Inert gas is pumped into the bubbler at a measured rate so that it bubbles through the liquid from bottom to top. Vapor constituents of the gas over the surface of this liquid is in equilibrium with the liquid at the measured temperature. The amount of metal containing vapor fed into the reactor is then a function of the measured temperature, pressure, and initial gas flow rate. For a three component film as (Cd, Zn)Te, there are over 15 variables to optimize for good films.

Epitaxial CdTe layers were initially grown on GaAs substrates by MOCVD to establish basic growth conditions. Dimethylcadmium (DMCd) and dimethyltellurium (DMTe) were used as Cd and Te sources, respectively. During the growth process, substrate temperature was varied over 380 to 440 °C, and the DMTe/DMCd ratio was varied from 1 to 5. A maximum growth rate of approximately 25 µm per hour was demonstrated.

The resulting CdTe/GaAs samples were then characterized for morphology, thickness, and crystal quality. Mirror-like morphology was obtained for a substrate temperature of 420°C and VI/II ratio of 3. Figure 6 shows optical microscope photographs of CdTe/GaAs sample grown to 8 µm using a 16 µm per hour growth rate. The thickness of the CdTe layer was determined from infrared reflectance measurements which are presented in Figure 7. X-ray diffraction measurements were also performed to assess the structural quality of the film. Figure 8 shows a [333] X-ray reflection from the 8 µm thick CdTe sample, and a FWHM of 90 arc-second was obtained. In spite of the large lattice mismatch between CdTe and the GaAs substrate, the FWHM value suggests excellent crystal quality. The growth of CdTe on GaAs substrates was successfully used to determine optimum growth conditions.

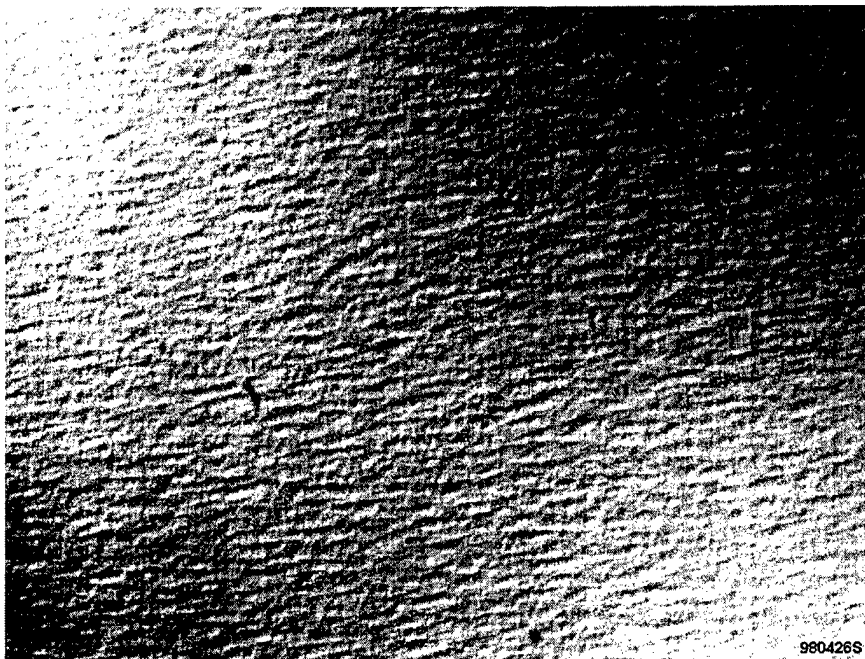


Figure 6 Surface morphology of CdTe grown by MOCVD on GaAs substrate, run #M4-4530 400x.

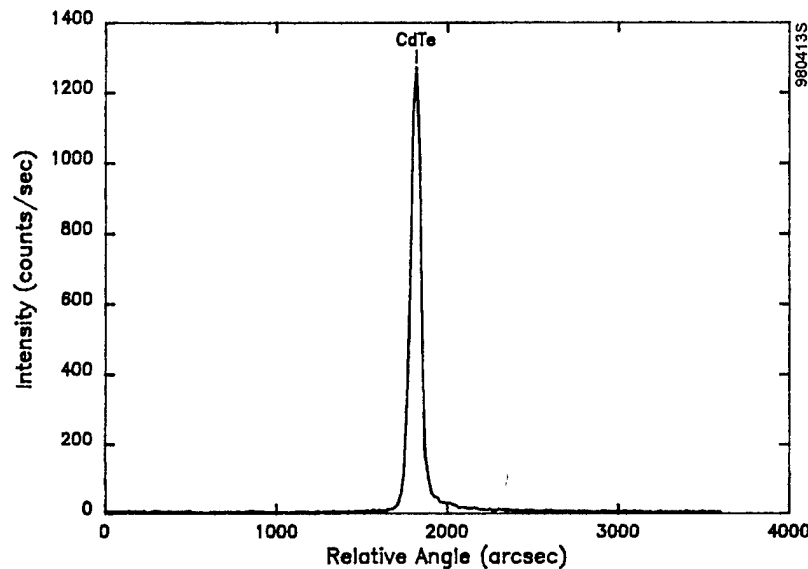


Figure 7 Double crystal X-ray diffraction data for a thick ($>50 \mu\text{m}$) CdTe layer on GaAs.

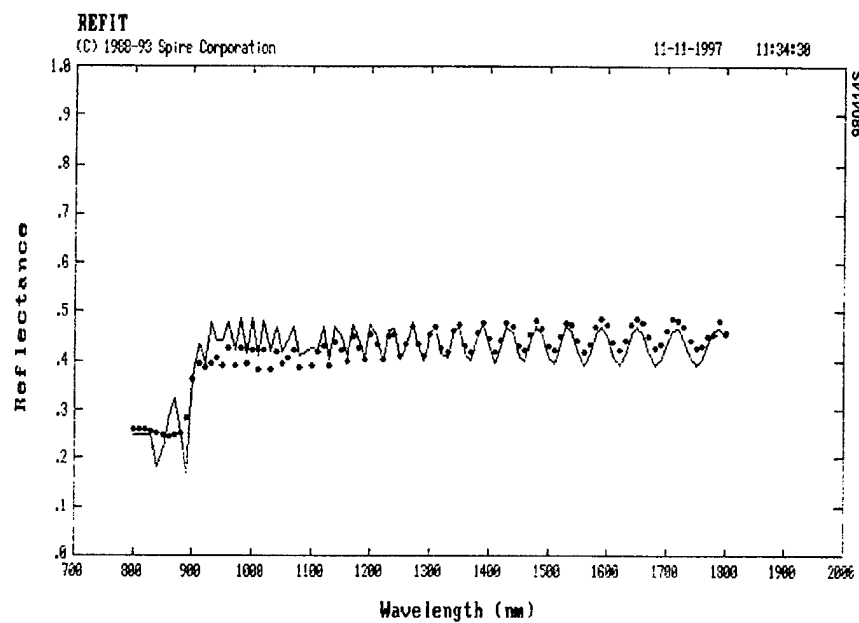


Figure 8 Infrared reflectance as a function of wavelength (nm) for CdTe layer grown by MOCVD on GaAs substrate. Sample #MO-4495-1.

CdZnTe layers were first deposited onto Corning 7759 glass substrates by MOCVD using a Spire 3000GTM MOCVD reactor. We varied the VI/II gas ratio in the mixture over the range 0.3 to 1.5. We also varied the Zn composition over the range 0 to 30%. The resulting thin films were then characterized for thickness, composition, and sheet resistance. Film thickness in the range 0.6 μm to 1.5 μm was determined using Alpha-step measurements. Optical transmission measurements from 300 to 1100 nm were performed to determine Zn composition, and the

resulting transmission data are presented in Figure 9. The band-edge absorption is clearly visible for two CdZnTe samples grown with 18% and 28% Zn compositions. The data clearly indicate an expected band-edge shift toward shorter wavelengths. At room temperature, the bandgap of CdTe is 1.5 eV, or approximately 820 nm. The Zn composition (x) can then be determined from the measured bandgap of CdZnTe using the equation:

$$E_g = 1.51 + (0.606)x + (0.139)x^2$$

It is clear from the sheet resistance data that initial CdZnTe thin layers do not have sufficient resistivity to achieve the required low leakage current.

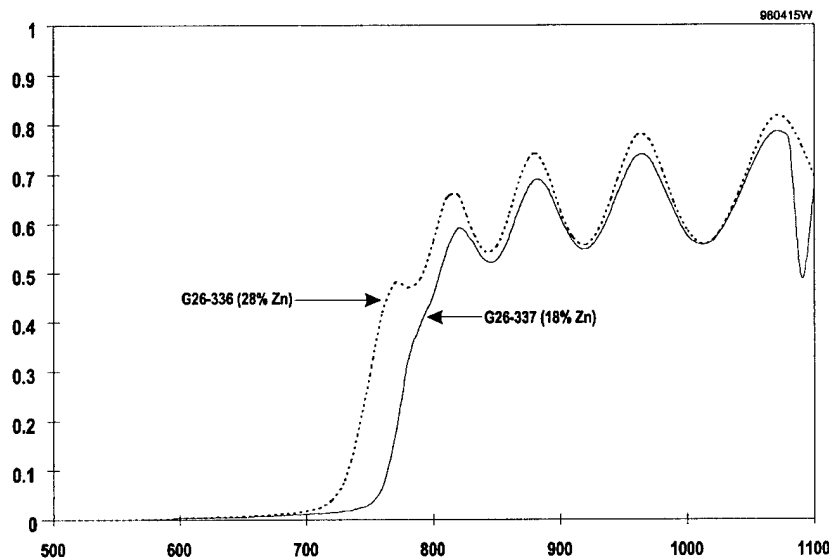


Figure 9 Room-temperature transmission data for CdZnTe thin film deposited on glass substrates by MOCVD.

Table 4 Sheet resistance data of CdZnTe layers deposited by MOCVD.

Sample ID	Zn Comp (%)	II-VI Ratio	Thickness (μm)	Voltage (Volts)	Current (Amps)	R (ohms)	R _n (ohms /sq)
336-1A	28	1.5	1.57	100	2.48E-08	4.03E+09	3.67E+11
337-1A	18	1.5	1.53	100	1.77E-08	5.65E+09	5.14E+11
337-1B	18	1.5	1.53	100	4.43E-08	2.26E+09	7.77E+11
338-1A	0	0.5	0.9	100	2.81E-08	3.56E+09	3.24E+11
338-1B	0	0.5	0.9	100	2.84E-07	3.52E+08	1.21E+11
339-1A	0	0.3	0.6	100	1.18E-08	8.47E+09	7.71E+11
339-1B	0	0.3	0.6	100	5.72E-08	1.75E+09	6.01E+11
340-1A	30	0.5	0.8	100	3.29E-08	3.04E+09	2.77E+11
340-1B	30	0.5	0.8	100	6.66E-08	1.50E+09	5.17E+11

Film thickness and deposition temperature are closely interrelated, the higher the temperature the faster the deposition rate and lower the process cost. However, the maximum deposition temperature is closely tied to choice of substrate. CdSe TFTs, no longer available,

can withstand higher temperatures (typically 350°C) compared to amorphous silicon (a-Si) which is limited to about 250°C. Crystalline silicon circuits could withstand even higher temperatures, over 440°C. These factors prompted a series of MOCVD growth runs to examine the effects of growth temperature on film properties and growth rate.

Shown in Table 5 are results of a series of CdTe runs deposited on single-crystal GaAs substrates designed to examine deposition rate and film properties (principally, physical quality). These runs were all performed under similar conditions (pressure, VI/II ratio, absolute flow rates, *etc.*). It is apparent from these results that acceptable growth rates (>8 $\mu\text{m}/\text{hr}$) can occur under all conditions within the boundaries of these experiments. Film quality as determined by both physical appearance and X-ray crystallographic analysis (FWHM of X-ray peak) was also good, with preference towards the higher temperatures.

Table 5 **Summary of a series of CdTe MOCVD runs conducted at 500 torr pressure, VI/II=2.9, using dimethylcadmium (DMCd) and dimethyltellurium (DMTe). All films were deposited on semi-insulating GaAs substrates (2° off 100 orientation).**

Run No. (M4-)	Growth Temp. (°C)	Time (min.)	Thickness s (μm)	Rate ($\mu\text{m}/\text{hr}$)	X-ray FWHM (arc sec)	Physical Appearance
4497	380	30	4.3	8.6	288	slight haze
4493	400	30	5.6	11.3	144	good
4495	420	30	7.0	14.0	90	excellent
4500	440	30	7.2	14.3	180	excellent

It is known that film deposition rate and minimum growth temperature also depend on the particular MOCVD starting materials (precursors) that are used. For the runs indicated in Table 5, the tellurium source was DMTe (dimethyl tellurium). Other sources have been developed, and selected ones are listed in Table 6. DMTe has been used for most of our experiments because of its availability, purity, and relative low cost. However, it may not be the best choice for low-temperature growth of tellurides. A tellurium precursor with better low-temperature growth potential is diallyl telluride (DATE) which is also listed in Table 6. The main disadvantage of DATE is its higher cost (\$48/g) which is due primarily to low demand. CdTe has been successfully grown using DATE for HgCdTe infrared sensor substrate applications at temperatures as low as 240°C, but with relatively slow growth rates (only 0.6 $\mu\text{m}/\text{hr}$).¹⁷ While MOCVD growth of CdTe has been demonstrated at temperatures as low as 220°C using ditertiarybutyl tellurium (DTBTe),¹⁸ DTBTe is currently not commercially available.

Table 6 Properties of selected tellurium precursors (Ref.19).

Precursor	Abbreviation	Vapor Pressure (torr @ °C)	Demonstrated Growth Temperature	Cost (in 500g quantity)
Dimethyl tellurium	DMTe	51.9 @ 25	500	\$33/g
Diethyl tellurium	DETe	9.3 @ 25	450	Not commercially available
Diisopropyl tellurium	DIPTe	5.6 @ 30	350	Not commercially available
Diallyl tellurium	DATe	3.3 @ 40	240 (Ref. 13)	\$48/g
Ditertiarybutyl tellurium	DTBTe	4.3 @ 50	220 (Ref. 14)	Not commercially available

Shown in Figure 10 are data showing MOCVD growth rate of CdTe on glass, ITO-coated glass, or CdS/ITO-coated glass substrates as a function of deposition temperature. Some of these data are from this program, some are from an ongoing related commercial program at Spire. A variety of growth conditions are included (e.g., specific precursors, VI/II ratio, pressure, absolute flow rates, *etc.*) resulting in the scatter of data at higher temperatures. The important points, however, are: 1) the growth rate increases with temperature, and 2) slow, but reasonable, growth rates are possible at temperatures as low as 250°C. These have important ramifications for this program, namely that reasonable growth can be expected in the 350°C temperature range which is that needed for deposition onto CdSe TFT arrays.

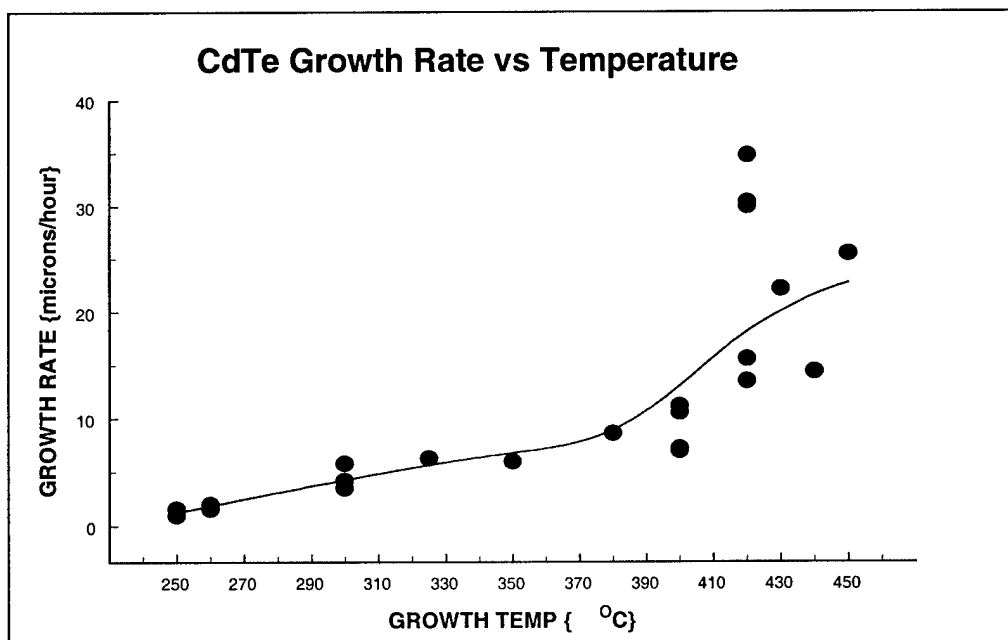


Figure 10 Growth rate for MOCVD-deposited CdTe as a function of temperature.

Another important requirement for the deposited films is that they possess good surface morphology and smooth surfaces, particularly for thicker films (>100 µm). Formation of particulates within the growth chamber and their falling onto the substrate during growth can be

especially problematic. Early growth runs often suffered from this problem as demonstrated in Figure 3. This profilometer plot shows a surface scan for a CZT thin film (approximately 5 μm thick) deposited on an ITO-coated glass substrate; surface features approximately equal to the film thickness are apparent.

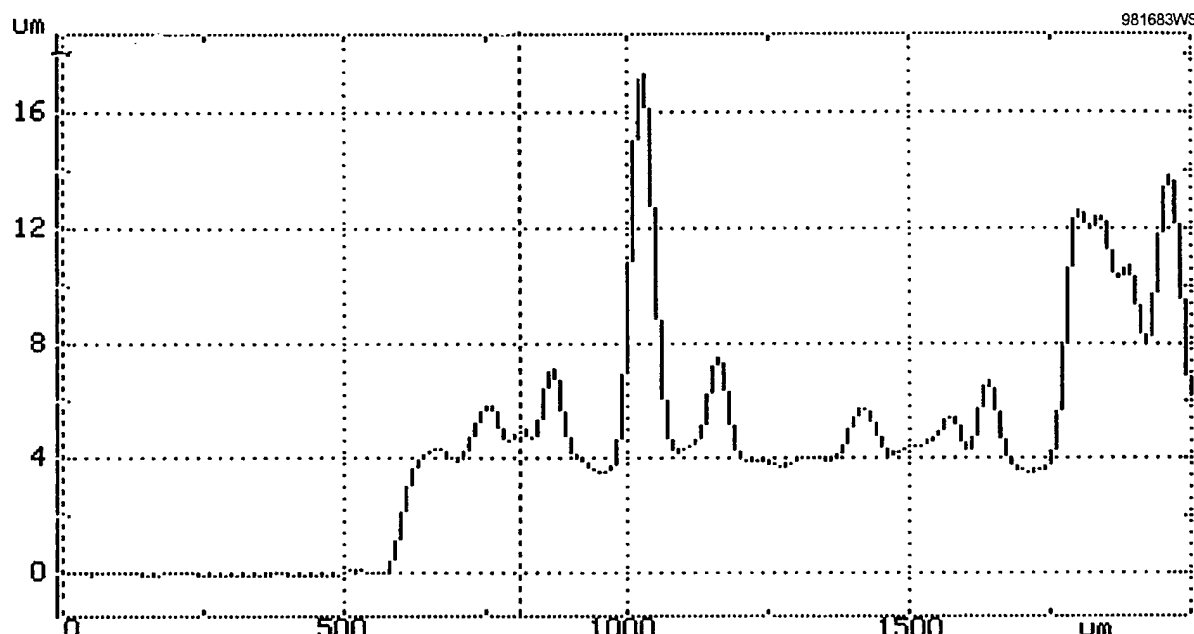


Figure 11 Profilometer plot of a CZT film (M4-4549) deposited on an ITO-coated glass substrate using a flat susceptor.

During growth of films such as that in Figure 11, the glass, ITO-coated glass, or CdS/ITO-coated glass substrates (typically 1-2 mm thick) have sat horizontally on an rf-heated, flat graphite susceptor. Since the injected gases flow vertically downward, the opportunity exists for small eddy currents to form near the substrate edges which can lead to CdTe particle formation and subsequent deposition onto the substrate. If these deposits form early in the growth process, they can act as nuclei for further growth and thus lead to larger particles which result in a very rough surface. To solve this problem, we replaced the flat susceptor with a “pocketed” susceptor with recesses machined into the susceptor top surface that were the same size, shape, and depth (thickness) as the glass substrates, thus resulting in a growth surface which was essentially planar with no features. Results of growth of a similar thickness film using the new susceptor appear in Figure 12. Compared to the film shown in the previous figure, this film is clearly superior in its surface smoothness.

Materials studied during this program include both CdTe and CdZnTe (CZT). CZT has the advantage that the addition of Zn to CdTe raises the bandgap and increases the resistivity. However, the X-ray absorption is slightly decreased because Zn ($Z=30$) has a smaller atomic number, Z , than Cd ($Z=48$). The net result of these counteracting effects is that there is an optimum Zn concentration which is usually in the 10 to 20 mole percent range.

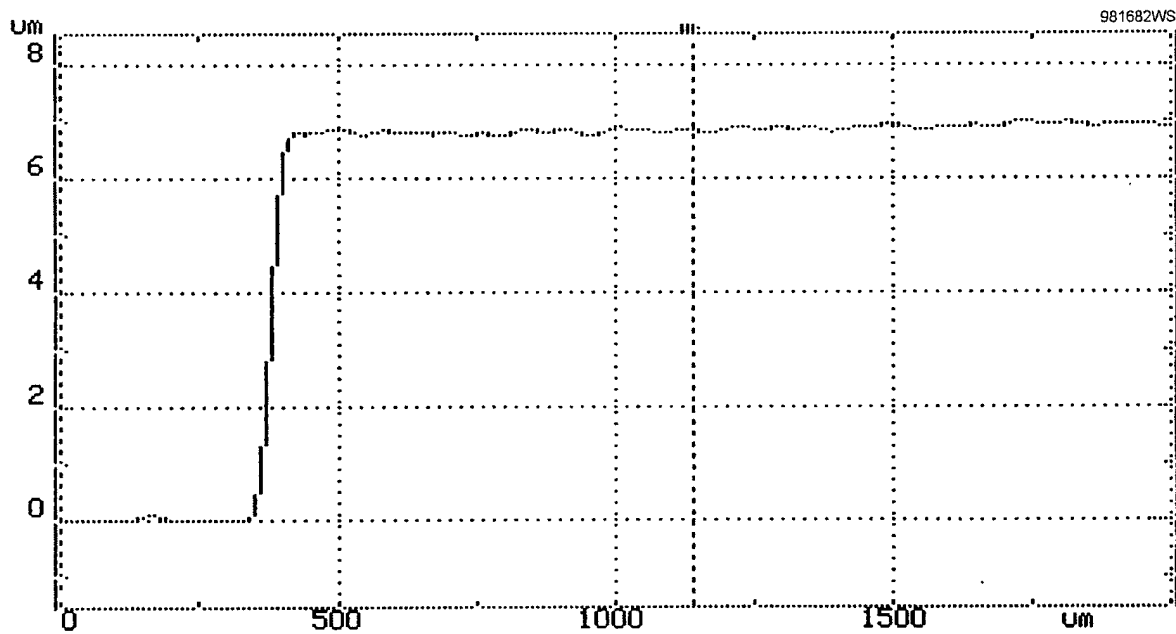


Figure 12 Profilometer plot of a CZT film (M4-4632) grown using a “pocketed” susceptor.

Summarized in Table 7 is a series of runs performed to study the effects of Zn incorporation in CZT films. All films were deposited on ITO-coated glass substrates under the conditions noted in the Table, and Zn concentration of the Cd_{1-x}Zn_xTe was determined from optical transmission measurements to determine the bandgap, E_g, which is uniquely related to Zn concentration, x, through the empirical relationship

$$E_g(x) = 1.51 + (0.606)x + (0.139)x^2. \quad (1)$$

The bandgap is estimated by extrapolating the linear region of the band edge to the ordinate.

Table 7 Summary of MOCVD experiments aimed at studying Zn incorporation. Zn concentration was determined from optical transmission measurements.

Run No.	Growth Temp (C)	DMCd Flow (sccm)	DEZn Flow (sccm)	Cd/Zn Ratio	DMTe Flow (sccm)	VI/II Ratio	Zn conc.
4533	420	155	75	2.07	375	2.92	0.00
4536	420	100	100	1.00	290	2.97	0.00
4537	420	75	100	0.75	240	2.98	0.00
4542	420	60	150	0.40	145	1.71	0.08
4541	420	40	100	0.40	100	1.77	0.28
4545	430	40	100	0.40	100	1.77	0.28
4544	440	40	100	0.40	100	1.77	0.40
4539	420	30	100	0.30	100	2.02	0.40
4540	420	20	100	0.20	120	2.81	0.57
4535	420	0	100	0.00	87	3.01	1.00

1.3.3 Low-Temperature Deposition

Since CdSe TFT arrays are no longer available, and a-Si:H TFTs are one alternative, we performed a series of experiments to determine whether adequate growth rate and film quality could be achieved at a growth temperature of 250°C - the maximum to which a-Si:H can be subjected without rapid degradation. These experiments were funded by a commercial customer at no cost to this program. We include the results here to present a more complete picture of current status and future prospects for CdZnTe thin-film x-ray detectors.

In order to improve the growth rate at low temperature, an alternative tellurium source, diallyltellurium (DATE) was used in place of the usual dimethyl tellurium (DMTe). Even so, the growth rate was an order of magnitude lower than typically achieved at 400-450°C. Furthermore, the resistivity of the films was much lower than at higher growth temperature. A number of different growth conditions were used, and films were deposited both on ITO and on CdS/ITO, the latter forming a heterostructure which often provides lower leakage current. The salient results are summarized in Figure 14, which gives the resistivity as determined by I-V measurements for CdZnTe/ITO films and the leakage current for CdZnTe/CdS/ITO. Unfortunately, the resistivity tends to decrease as the growth rate increases. There is no clear trend for the leakage current of CdZnTe/CdS/ITO as a function of growth rate.

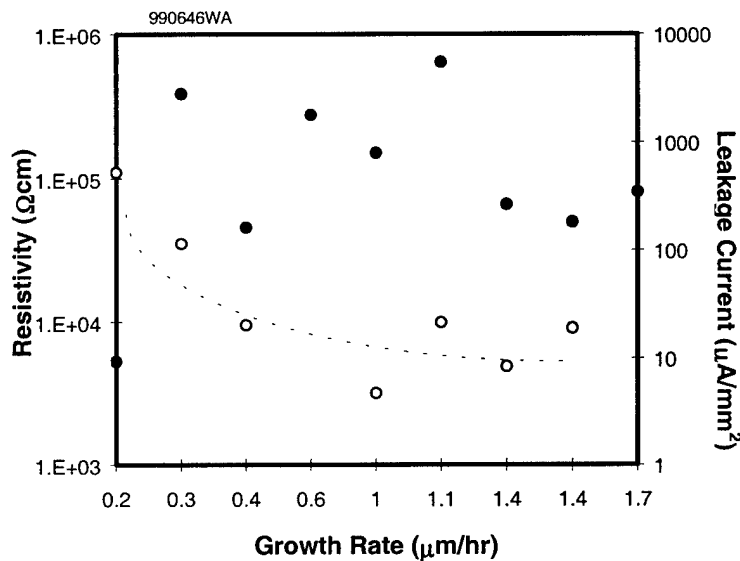


Figure 13 Resistivity as determined by current-voltage measurements for CdZnTe/ITO (open circles) and leakage current for CdZnTe/CdS/ITO (closed circles) versus growth rate at 250°C.

The conclusion that must be drawn from these experiments is that both the growth rate and the electrical properties of the films grown at 250°C are unacceptable. Hence deposition of CdZnTe films on a-Si TFTs by MOCVD appears not to be practical.

1.3.4 High-Temperature Deposition

We conducted a number of runs at a temperature of 420-440°C using DATE as the Te source. This precursor gives poor growth rates in this temperature range, typically 1-3 $\mu\text{m}/\text{hr}$. Experiments reverted to dimethyl tellurium (DMTe), which gave much higher growth rates, approximately 15 $\mu\text{m}/\text{hr}$ for CdTe, but somewhat lower for CdZnTe. A series of runs were performed varying the VI/II flow ratio.

Our previous results have shown that the electrical properties of the films may depend strongly on the alloy composition. In particular, higher resistivity is often obtained with Zn-rich films. It was important therefore to understand how the composition and growth rate depend on the flow rates of the precursors. To characterize this property we carried out several runs at fixed Cd and Zn flow rates while varying the Te flow rate. The temperature was fixed at 420°C.

Table 8 summarizes the results of both the high-temperature and low-temperature runs. In many cases, electrical measurements were not possible because the film failed to adhere to the substrate. It has not yet been determined whether this problem is due to high particulate or contaminant levels in the reactor or to degradation of the substrates in storage.

1.4 Tasks 2, 3 and 4 - Passive Matrix Test Structure

The as-deposited films exhibited leakage current too high for photoconductive X-ray detection. As an initial attempt to solve this unexpected problem, we developed a heterojunction diode structure using CdTe/CdS layers. The structure is a well known heterojunction used for solar cell applications, and it is known to exhibit very low leakage current. An electronics test setup was developed for radiation testing of the device, and an alpha source was used to demonstrate that the CdTe/CdS device is suitable for X-ray detection.

To evaluate the feasibility of a CdTe photodiode structure, we considered the I-V characteristics of a CdTe/CdS heterojunction which is known to have low leakage current. For this purpose, we obtained CdTe/CdS samples grown on glass substrate from the National Renewable Energy Laboratory (NREL). The structure is illustrated in Figure 15. The 20 µm CdTe layer was deposited by close-spaced sublimation method over a CdS layer on ITO contact. Because the deposition process used by NREL has been optimized for 5 µm CdTe layers for solar cell devices, it is not clear that this 20 µm device exhibits the lowest possible leakage current characteristics for our application. Further work is required to optimize this aspect of the design. A gold ohmic contact was then applied to the CdTe p-layer for test purposes.

I-V characteristics of the device were measured using an HP4145A semiconductor parameter analyzer, and the results are presented in Figure 16. A leakage current of approximately 50 nA for a 3 mm diameter contact was obtained at a reverse-bias voltage of -25 volts.

In order to further evaluate the CdTe/CdS heterojunction as a potential X-ray detector, we performed alpha particle measurements using the test setup illustrated in Figure 16. A single gold contact layer was deposited on the top CdTe layer for ohmic contact, and the device was reverse biased over the range 25V to 45V. A straightforward electronics readout system was set up as shown. The device was then irradiated from the top with an alpha source to measure the detector response. The diode junction is formed deep within the device between the CdTe and CdS layers, and depletion occurs upward into the CdTe layer as the device is reverse biased. A response arising from alpha interactions close to the surface is then a clear indication that the depletion has extended sufficiently far into the CdTe layer to achieve good charge collection properties throughout the device. This charge collection throughout the CdTe layer is required for efficient X-ray detection. The response of the system to alpha radiation is presented in Figure 17. For bias levels less than approximately 30V the detector response is negligible. Above 35V, however, a significant response is obtained suggesting that the device is being sufficiently depleted at this bias level. These results are very promising, and lead us to believe that the CdTe/CdS structure will serve as a good X-ray detection medium for this application.

Table 8 MOCVD Growth Parameters and Film Characteristics

Structure	Substrate Temp (°C)	VI/II Ratio	Zn (Zn+Cd) Flow Ratio	Growth Rate ($\mu\text{m/hr}$)	Te Source	[Zn]	I(CdS) (nA)	I(ITO) (nA)
CdTe	420	0.7	0	17.1	DMTe			
CdTe	250	0.5	0	1.2	DATe			
CdZnTe	250	0.5	0.295		DATe			
CdTe	250	0.3	0	1.2	DATe			
CdZnTe	250	0.1	0.538	2.0	DATe			
CdZnTe	250	0.8	0.627	1.2	DATe			
CdZnTe	250	0.6	0.618	1.3	DATe			
ZnTe	250	0.3	1.0	0.2	DATe			
CdZnTe	250	5.6	0.622	1.0	DATe			
CdZnTe	250	1.7	0.606	0.5	DATe			
CdTe	440	1.1	0	1.6	DATe			
CdZnTe	440	0.4	0	0.6	DATe		N/A	22,000
CdTe	440	0.4	0	1.2	DATe		9.1	3.7×10^6
CdTe	440	0.4	0		DATe		180	N/A
CdTe	440	0.4	0	5.5	DATe			
CdTe	440	0.5	0		DATe			
CdTe	440	0.4	0		DATe			
*CdTe	440	0.8	0	0.7	DATe			
CdTe	420	0.7	0	17.7	DMTe			
CdTe	420	0.7	0	16.2	DMTe			
CdTe	420	0.7	0	17.0	DMTe			
CdZnTe	420	1.0	0.677	13.2	DMTe	0.59		
CdZnTe	420	1.5	0.677	15.0	DMTe	0.49		
CdZnTe	420	3.0	0.677	17.0	DMTe	0.32		

* First run with rotating susceptor

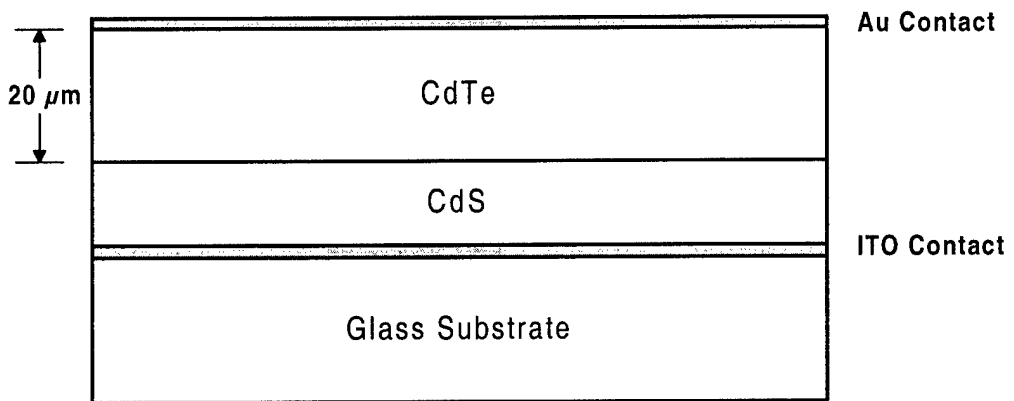


Figure 14 Illustration of CdTe/CdS heterojunction structure obtained from NREL.

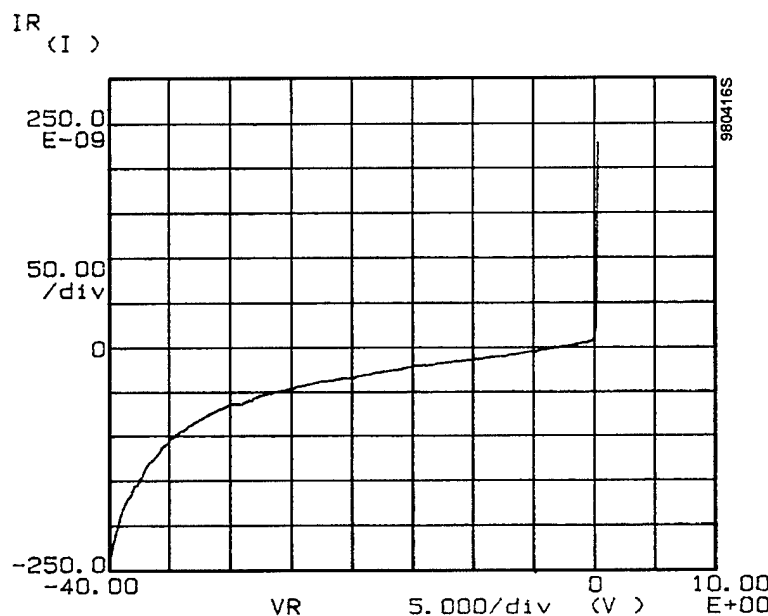


Figure 15 I-V characteristics of CdTe/CdS heterojunction structure obtained from NREL. The device shows improved leakage current performance over bulk thin-film material.

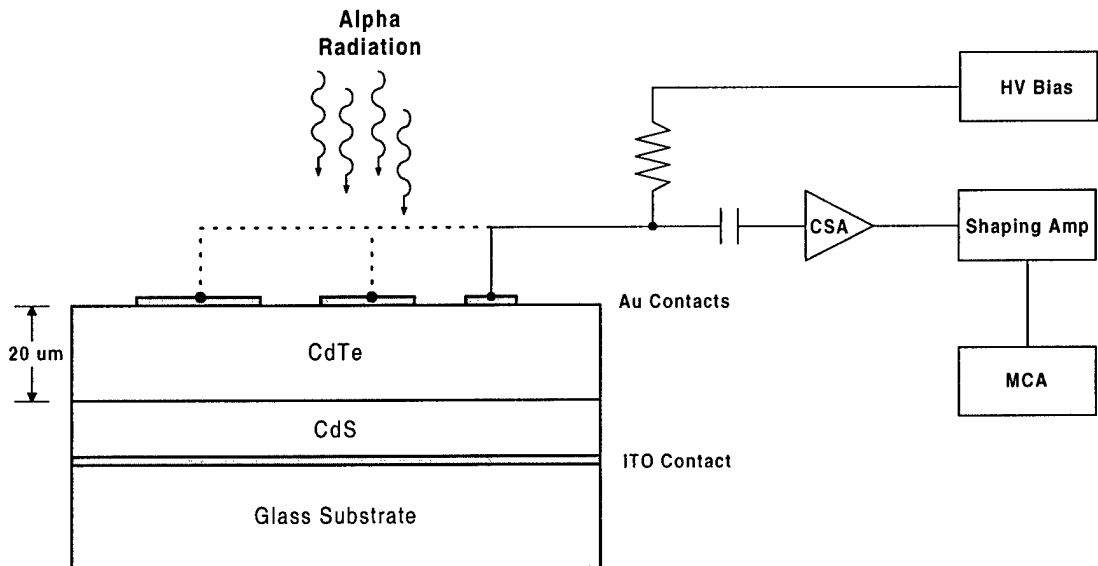


Figure 16 Schematic diagram of test setup used to evaluate CdTe/CdS heterojunction as a potential X-ray imaging detector.

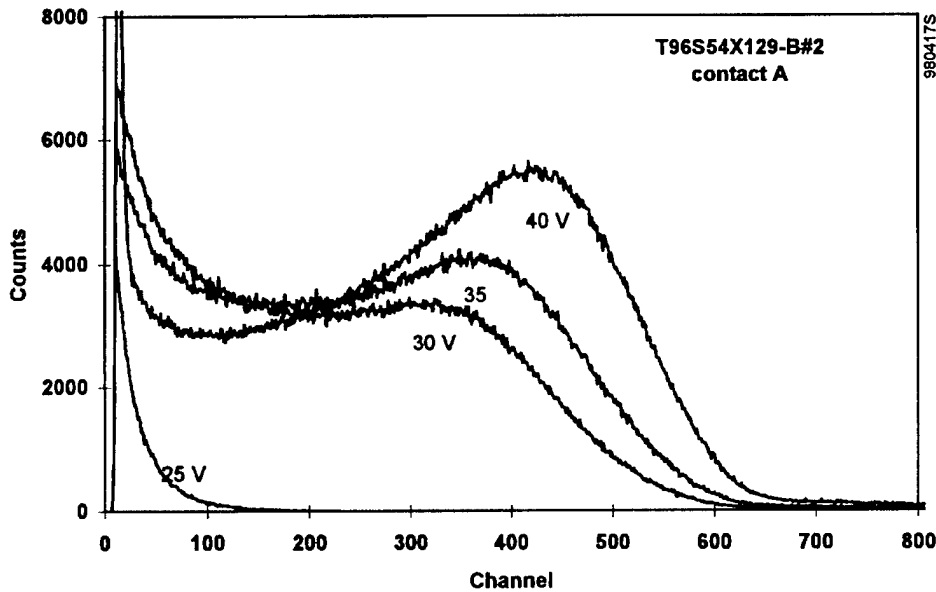


Figure 17 Response of CdTe/CdS solar cell structure irradiated with alpha particles.

Because the bulk CdTe and CdZnTe thin films exhibit insufficient resistivity, it is not practical to continue with the original plan to develop a passive matrix test structure. As an alternative we tried to repeat the test setup illustrated in Figure 16 with a variety of contact sizes and geometries. Unfortunately, film properties were further degraded when experiments had to be shifted to a different facility for safety reasons (technicians were exposed to fumes from the metalorganic sources) and working devices were not realized.

1.5 Task 5 and 8 - Model (Cd,Zn)Te Detectors for Mammography, Prepare to characterize Silicon Multiplexors with (Cd, Zn)Te : work performed by Dr. Rowlands, subcontractor

The first phase of the project was to theoretically investigate the advantages, and disadvantages of CZT compared to amorphous selenium and then to analyze the different approaches to digital radiography in general and digital mammography in particular.²⁰ We developed computer models of the imaging properties of photoconductor layers including all relevant parameters of the active matrix array. Using the model, we calculated the following three parameters as a function of spatial frequency: modulation transfer function, noise power spectrum and the derived quantity – the detective quantum efficiency. The calculations were novel in that they included specifically two important effects: (i) K-fluorescence escape and reabsorption and (ii) trapping of carriers in the photoconductor bulk and at layers intentionally incorporated to limit current injection from the contacts.²¹ The model was tested and validated by computing in two independent manners (analytically and using Monte Carlo code) and then comparing with measurements from the literature. The novel part of this work compared to our earlier work was the incorporation of spatial frequency dependent effects.²²

Time-of-flight methods were developed for the measurement of mobility, lifetime and hence range of carriers in CZT. The approach depends on the availability of suitable samples of photoconductor. These have to have electrodes with good blocking contacts on either side. One electrode is transparent and after biasing the sample using the electrodes, a brief burst of highly absorbed light is incident on the transparent electrode. The freed carriers move as a sheet through the semiconductor and the time for the leading edge of the resulting current pulse to reach the other end of the sample is the time of flight. The lifetime of the carriers is established by noting the exponential decay of the current pulse as it passes through the layer. The apparatus was tested experimentally using Xerox amorphous selenium samples as shown in Figure 18.

An approach to measuring the sensitivity of photoconductors which also permits the measurement of the detection efficiency of CZT layers and their signal to noise ratio was developed which depends on the use of a lock-in amplifier. This apparatus was validated by use of a camera tube containing amorphous selenium but can also be used with dual electroded samples of any photoconductor.

Methods were developed to measure the time response of photoconductive layers to radiation. The principle of the methods was to use the very fast pulses from a clinical linear accelerator (linac) to excite a short x-ray pulse in the sample. The resulting current from an electroded sample was measured with an oscilloscope. Typical results using an amorphous selenium sample are shown in Figure 19 which demonstrates the motion of the holes as the first high amplitude short duration pulse followed by the smaller amplitude but longer electron pulse.

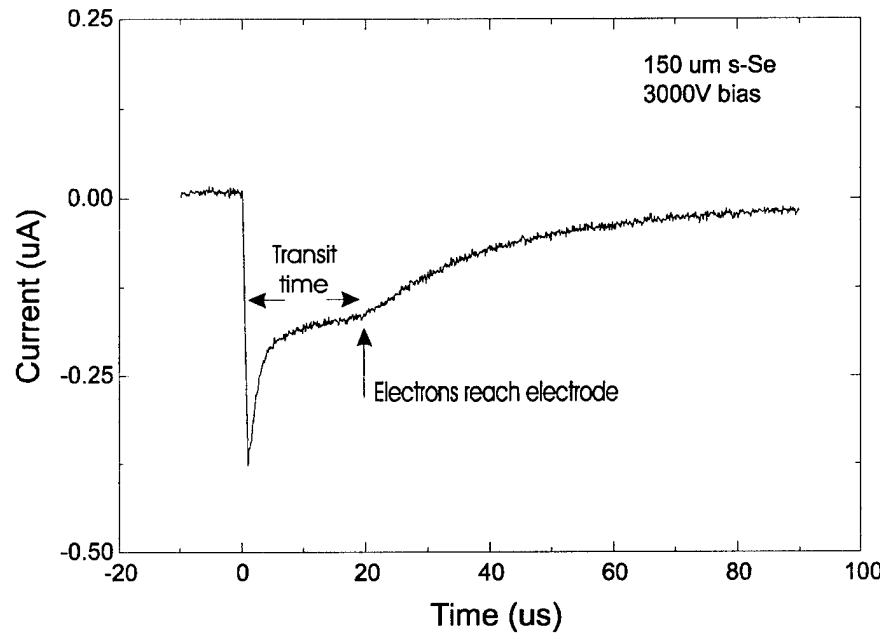


Figure 18 Electron time of flight in an amorphous selenium sample.

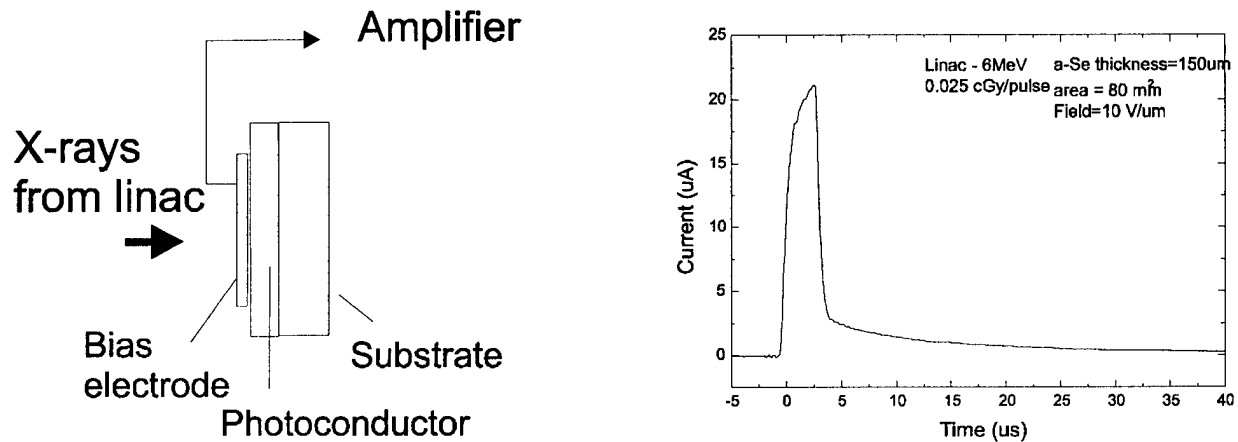


Figure 19 Apparatus for the measurement of the time response of electroded samples and the response of an amorphous selenium sample to a 2 : s radiation pulse from a linac.

We designed measurement techniques for CZT samples and tested them with available samples of *amorphous selenium*. The techniques we developed for this project were xerographic discharge methods for non-electroded samples, and for electroded samples time-of-flight measurements, pulse height methods for measuring the x-ray to charge conversion efficiency and the Swank factor²³ for determining the zero spatial frequency detective quantum efficiency. There are unavoidable fluctuations in the signal produced in the detection medium even when x rays of identical energy interact and produce a response. These fluctuations are caused by the statistical nature of the competing mechanisms that occur as the x ray deposits energy in the medium. Together these effects give rise to a category of noise known as *gain-fluctuation noise*.

The first discussion of gain-fluctuation noise and estimates of its magnitude, in the context of x ray detection with phosphors, was given by Swank.²⁴ The gain-fluctuation noise is experimentally determined using the *pulse height spectrum*, or PHS, obtained using monoenergetic x-ray sources as shown in Figure 20 for photoconductors. Monoenergetic x rays are incident on the detector, one at a time, and the quantity of charge , released directly by a photoconductor or indirectly (by interaction of the released light with a photocathode of a photomultiplier) by a phosphor is measured. This is performed using a pulse shaping circuit that has the property of integrating the charge from the photoconductor (or photomultiplier if using a phosphor) into a pulse whose height is proportional to the integrated charge. The multichannel analyzer then digitizes the pulse height and increments a counter corresponding to that height. This creates a histogram called a PHS. This can be interpreted, and if necessary calibrated using a *charge terminator* as shown in Figure 4(b), in terms of charge or deposited x-ray energy.

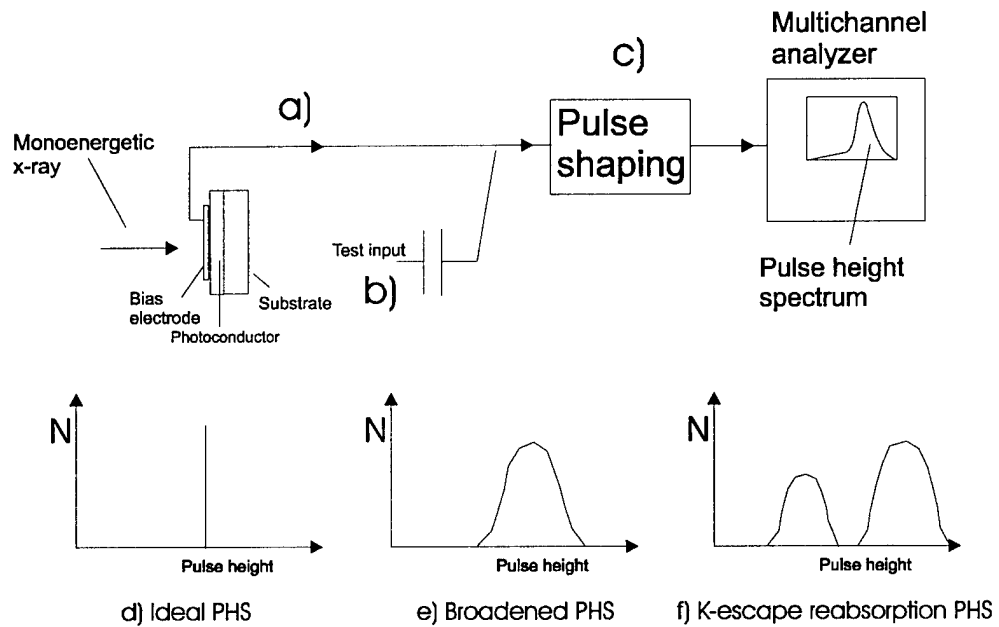


Figure 20 **Measurement of pulse height spectra of photoconductor layers and examples of spectral broadening due to several physical effects (e) broadening due to trapping in the photoconductor layer $A_s \sim 0.9$, (f) broadening of the spectrum due to escape and partial re-absorption of K-fluorescent x-rays, $A_s \sim 0.7$.**

Prototypical pulse height spectra are shown in Figure 20. In (d) is the ideal spectrum – all x rays give rise to equal amounts of charge, resulting in a delta function. This, as shown in the caption, has a value of the Swank factor $A_s=1$. Other possible shapes due to statistical broadening, K-fluorescence escape, and optical broadening²⁵ due to absorptive bulk dye or backing will have the form shown, and the corresponding, approximate value of A_s is given in the caption to Figure 4. Such measurements and related theoretical estimates have been performed for a range of detection media including the phosphors $\text{Gd}_2\text{O}_2\text{S:Tb}$,^{26,27} CsI:Na ,²⁸ and for layers of stabilized *amorphous selenium*.^{29,30} The noise due to both quantum absorption inefficiency and gain fluctuations can be combined to create the *zero spatial frequency detective quantum efficiency* $DQE(0)$ that is given by: $DQE(0) = A_Q A_S$ where A_S is the correction due to gain fluctuation noise and can be expressed in terms of the moments of the PHS. The energy of

the incident x ray is important since above the K-edge of the material, K-fluorescence escape can significantly affect the distribution of measured signals and reduces the Swank factor, representing an increase in Swank noise. Higher Z materials with K-edges in the range of energies present in a diagnostic x-ray beam will exhibit more image degradation due to this mechanism than lower Z elements whose K-edge is at lower energies. However, changes in the absorption coefficient across the K-edge can also make these higher Z materials less sensitive, on average, to the lower energy scattered radiation produced in the patient.³¹ For the specific case of mammography we found CZT to be superior to amorphous selenium as there is no K-fluorescence due to the low energy of the monographic spectrum compared to the K-edges of the major radiographic constituents of CZT. Taken together these measurement and modelling techniques permit us to understand and predict the behaviour of flat panel detectors from the basic measurements taken from samples of photoconductor.

For the next stage of measurement, MTF of photoconductive layers was made using fully functional imagers with a very fine pixel pitch to closely match the requirements of a mammographic imager. We used commercially available 2-D multiplexer chips. These are complete imaging systems on an integrated circuit "chip" with a 2-D array of electrodes on its upper surface. (These chips were designed to permit an infrared sensitive array of photodiodes made from a small energy gap semiconductor to be "indium bump" bonded to the structure). For our application the use of the chips is even simpler - the photoconductor layer to be tested is formed by thermal evaporation directly onto the multiplexer. This is possible because the MOCVD process permits the substrate be kept at <300°C during the CZT layer formation. This is a relatively low process temperature for silicon chips thus the CZT layer can be formed directly onto the high purity silicon without any significant danger of damage to the multiplexer or compromise in the quality of the CZT layer. We used a 128 x 128 pixel high purity silicon multiplexer chip (with 50 µm x 50 µm electrodes) made by EG&G Reticon (RA0128M) shown in Figure 5.

Each multiplexer was tested by the manufacturer. The imaging performance of the arrays with a photoconductor evaporated onto it was evaluated using an *amorphous selenium* layer evaporated for us by Noranda Advanced Materials, Inc. It is planned that qualified arrays with a layer of CZT will be returned to Sunnybrook for imaging tests. Furthermore for samples evaporated onto silicon multiplexers it was necessary to build, construct and test a digital readout system compatible with this multiplexer.³²

For this purpose the arrays are connected to our real-time (30 frame per second, 12 bit A/D) imaging system. Data is acquired in digital form presampled MTF and uniformity of dark current and gain measured.

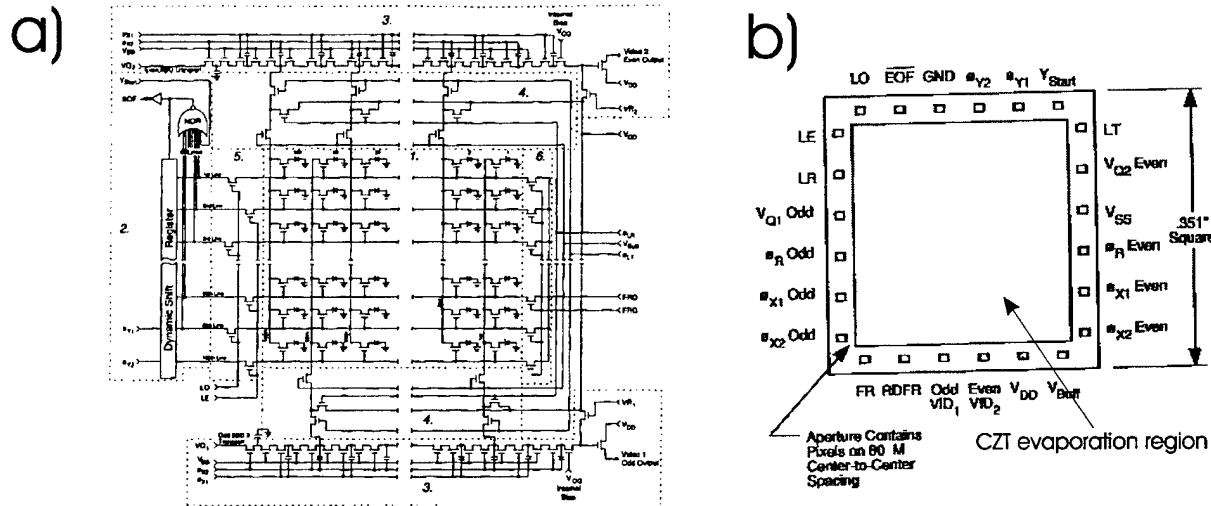


Figure 21 Schematic diagram of silicon multiplexer a) circuit diagram and b) plan view of top of multiplexer showing (black square) region where photoconductor is evaporated.

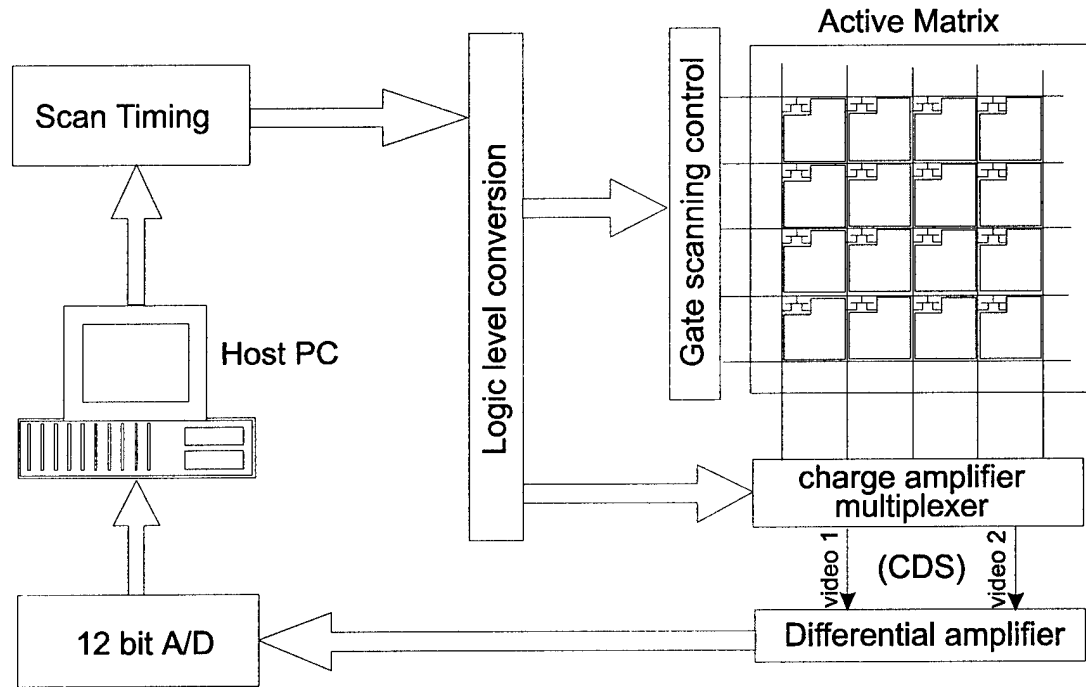


Figure 22 Modular readout system for flat panel imager described in text.

The final phase of the project was to prepare the measurement techniques in readiness for the supply of the flat panel active matrix arrays with CZT layers evaporated onto them. For this purpose a general-purpose active matrix readout system was designed, constructed, developed and optimised as shown in Figure 22. The design criterion was that the system could be used to

readout any design of active matrix array. This was required since while the readout system was being designed and built the supplier of the TFT array was not known. It was therefore decided that it should be capable of reading out any array from very small to very large arrays. Another important design criterion is was that the system should be reasonably priced and could be easily reproduced so that duplicate systems would be available at SPIRE and as well as at Sunnybrook. For this reason, the design was based on the use of generic PC systems and commercially available plug-in cards. We also used IDL as the programming environment to permit rapid and flexible image processing of the resulting images. Our design permits the readout of images from array of from 2×2 pixels to 4000×4000 pixels in size and for a 500×500 pixel panel the readout time was measured to be less than a second. The total cost of materials to reproduce a duplicate readout system was kept below the target of \$5,000 plus a PC.

1.5.1 Modeling of Absorption Efficiency

A typical x-ray spectrum used for mammography (50 kV, tungsten with 1.0 mm Be / 0.5 mm Al filter) is shown in Figure 6 both as it emerges from the x-ray tube and after attenuation by 5 cm of soft tissue.³³ While the spectrum that emerges from the tube is concentrated below 25 keV, the spectrum that reaches the detector is significantly hardened, so that the content between 30 and 50 keV makes a major contribution.

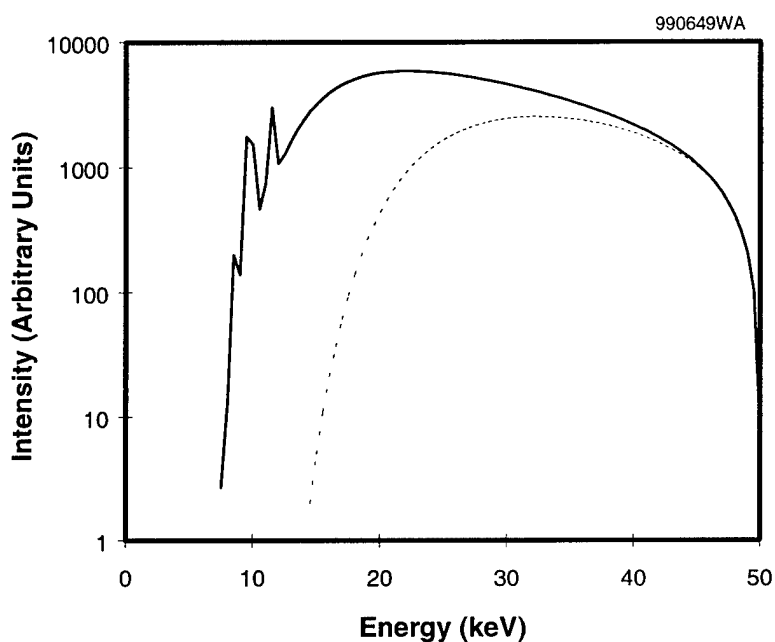


Figure 23 X-ray spectrum from a tungsten tube at 50 kV constant potential at the tube output (solid) and after attenuation by 5 cm of soft tissue (dotted).³⁴

We have calculated the energy absorption efficiency as a function of film thickness for these spectra using the equation:³⁵

$$\eta = \frac{\int_0^{\infty} (1 - e^{-\alpha(E)d}) g(E) E dE}{\int_0^{\infty} g(E) E dE}$$

where $\alpha(E)$ is the attenuation coefficient for photons of energy E , $g(E)$ is the spectral density plotted in Figure 6, and d is the detector thickness. The results are shown in Figure 7, both for CdTe and selenium. The horizontal axis is in units of g/cm^2 , so that the actual film thickness is obtained by dividing by the density of the material ($5.87 \text{ g}/\text{cm}^3$ for CdTe, $4.3 \text{ g}/\text{cm}^3$ for a-Se). CdTe has significantly higher absorption efficiency than a-Se for a given film thickness, especially for the spectrum as hardened by soft tissue absorption. The CdTe film thickness required for 90 % absorption efficiency is approximately $200 \mu\text{m}$, compared to more than $600 \mu\text{m}$ for a-Se. This result implies that the growth rates obtained by MOCVD in the $400\text{-}500^\circ\text{C}$ range ($\approx 10\text{-}20 \mu\text{m}/\text{hr.}$) are acceptable, but that the growth rate at 250°C ($\approx 1 \mu\text{m}/\text{hr.}$) is not practical for depositing films of sufficient thickness for x-ray detection. Similar calculations were performed for higher X-ray energies; results are given in Appendix A.

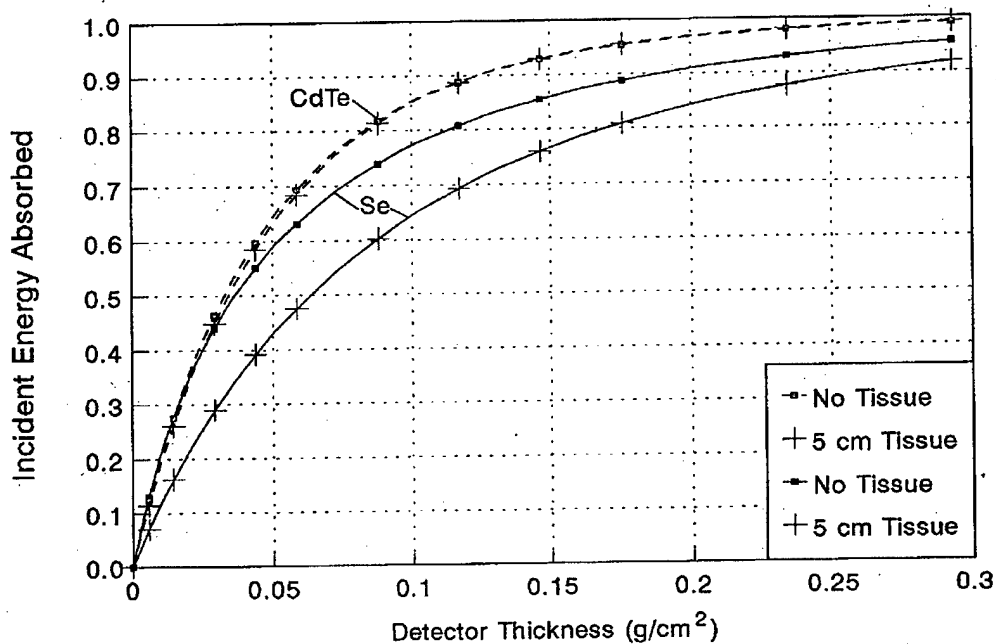


Figure 24 Absorption efficiency for x-ray spectra shown in Figure 23 as a function of film thickness for CdTe and Se.

1.6 Tasks 7, 10 and 11

In the last year of this program experiments were stuck on these two obstacles: (a) the detector material we could deposit in thin film form had too low a resistance for a radiation detector, and (b) the deposition temperature was too high for the readout potential customers had insisted upon using. We tried to address both of these problems to show the potential of the proposed approach.

Deposition runs were made to “clean-up” the reaction chamber. It was believed that residual contaminants were being evaporated from the chamber walls when heated and these doped the film being deposited. Successive attempts to clean the chamber, pre-coat the chamber, use pre-deposition runs did improve the resistance by about a factor of 50, but this was still not sufficient to fabricate a working device.

On a more positive note, we were able to show that new TFT technology based upon poly-crystalline silicon technology would survive high temperature deposition of (Cd, Zn)Te. Attempts to deposit films for measurements were not very successful in that detectors could not be fabricated with low resistance material-however, circuits exposed to the this film deposition functioned well afterwards. A very high temperature cycle was used. The substrate was pre-baked at 625°C for 400 seconds, then heated at 475°C for one hour during deposition.

Dr. Rowlands furnished silicon multiplexor (EG&G Reticon RA0128M-NAQ-011 Solid State Area Multiplexer Array). It was certainly believed that at this temperature the metallization would react and degrade. However, careful measurement showed that the responsivity was uniform across the entire (optical) detector. Figure 25 shows an image made with this device (neither calibrated and nor corrected for pixel-to-pixel variations) before and after exposure to the deposition thermal cycle demonstrating that functionality remained identical.



Figure 25 Optical images obtained using EG&G multiplexer before (left) and after (right) heat treatment as described in text. The image is of the fluorescent light bulb above the workbench and the non-uniformity of the image is due to the fact that no attempt was made to calibrate the imagers (i.e no dark and bright fielding). However the images show clearly that the device was not substantially damaged by the heat treatment.

Dr. Hatalis of Lehigh University furnished the silicon TFT's (Figure 26). They were fabricated on quartz in a plasma-enhanced CVD system. The TFTs were fabricated by first depositing 100nm of passivating oxide followed by 50nm of hydrogenated amorphous silicon. The wafers were then removed from the PECVD system and heated in a furnace at 620°C for 2 hours to crystallize the silicon film that becomes the active device layer. The crystal silicon is patterned by photolithography. This step is followed by deposition of another 100nm of silicon dioxide as a gate dielectric followed by 100nm of amorphous silicon as the gate electrode. The electrode is then doped by ion implantation and patterned by photolithography. Additional ion implantations were performed to form the n-type (phosphorus) and p-type (boron) source and drain regions (also, additional lithography was required). The ion implants were activated by heating at 700°C for 2 hours, which also crystallizes the remaining amorphous material. Additional 300 nm of passivating surface oxide was deposited, patterned to open up contact vias, then (patterned) aluminum metallization was deposited for contacts. This step was followed by heating in hydrogen at 300°C to passivate grain boundaries. Test devices included TFT arrays and a 19 stage CMOS ring oscillator.

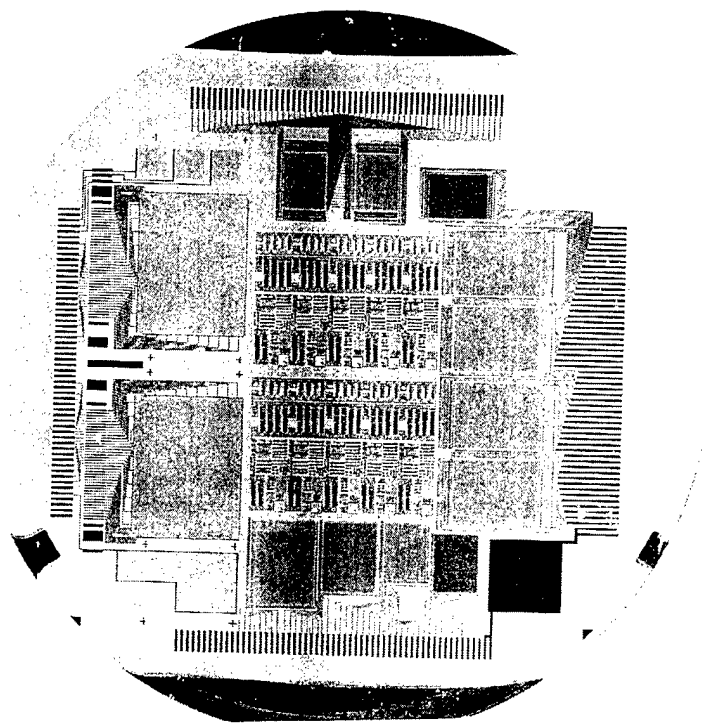


Figure 26 Picture of thin film silicon TFT circuit used to test CdZnTe detector. Outer region of wafer contains thin film transistor sensors, inner regions contains shift register.

All devices were characterized prior to deposition at Spire. All TFT's were functional with similar electrical characteristics. Their electron mobility was in the range of 8-14 cm²/Vs and their hole mobility was in the range of 4-8cm²/Vs. Threshold voltage of the n-channel device was between 6 and 11 volts, and 21 to 31 volts for the p-channel device.

After deposition of CdZnTe, the average electron mobility decreased from an average of 13.6 to 10.6 cm²/Vs and the threshold increased from an average of 9 to 22 volts. The p-channel

devices were less sensitive to the high temperature treatment. The threshold voltage changed by less than 1% and the mobility decreased from an average of 7.7 to 6.8 cm²/Vs. The ring oscillator had a gate delay of about 5ns, implying that the technology could support operating frequencies up to 180 MHz.

2 KEY RESEARCH ACCOMPLISHMENTS

- Demonstrated high deposition rates of (Cd, Zn)Te thin films
- Demonstrated controllable Zn compositions
- Demonstrated good crystal structure and surface morphology
- Demonstrated uniformity and repeatability of process
- Demonstrated that the process is compatible with new “crystal” silicon thin film transistor arrays
- Determined that the material electrical resistance was insufficient to fabricate x-ray detectors

3 REPORTABLE OUTCOMES

3.1 Publications

A list of publications of research work partly funded by this program is given below:

DC Hunt, W Zhao and JA Rowlands, “Detective quantum efficiency of direct, flat panel detectors for fluoroscopy” Medical Imaging 1998: Physics of Medical Imaging, Proc. SPIE 3336, 195-201 (1998)

JA Rowlands, “Current advances and future trends in x-ray digital detectors for medical applications”, IEEE Transactions on Instruments and Measurements, 47, 1415-1418 (1998)

JA Rowlands and SO Kasap “New Directions in X-ray Imaging” Proceedings of the 6th International Symposium on the Uses of Selenium and Tellurium, Scottsdale, Arizona, pp 25-35 (1998)

SO Kasap and JA Rowlands. “Photoconductor selection for digital flat panel x-ray image detectors based on the dark current”, Journal of Vacuum Science and Technology, A 18, 615-620 (2000).

3.2 Presentations

One presentation was given at the “ERA of HOPE” conference, June, 2000 , Atlanta GA. The abstract follows:

THIN -FILM CdZnTe DETECTOR ARRAYS*
FOR DIGITAL MAMMOGRAPHY

Nader M. Kalkhoran, Harvey B. Serreze, and Rengarajan Sudharsanan

Spire Corporation
Bedford, MA 01730

nkalkhoran@spirecorp.com

The most promising approach for improving diagnostic accuracy in x-ray mammography is replacement of film-based systems with digital x-ray imaging systems. Several manufacturers have introduced digital x-ray imaging systems employing amorphous silicon (a-Si) thin-film transistor (TFT) arrays in conjunction with phosphor screens or scintillator crystals that absorb x-rays and emit visible or near-IR light. A photodiode integrated with each TFT converts the light into an electrical signal. The next major step in the development of digital x-ray systems will be replacement of this two-step conversion process by a direct-conversion method, in which a photoconductor absorbs x-rays and generates an electrical signal directly. Several direct-conversion materials have been proposed, including amorphous selenium (a-Se), lead iodide (PbI_2), mercuric iodide (HgI_2) and thallium bromide ($TlBr$). Reasonable success has been achieved with each of these materials, but none has the combination of high resistivity and good carrier transport properties required for optimum detection efficiency.

Bulk cadmium telluride (CdTe) and cadmium zinc telluride (CdZnTe or CZT) have been shown to possess excellent x-ray absorption and carrier transport properties. We have undertaken a development program to investigate thin films of these materials deposited directly onto TFT arrays using a metalorganic chemical vapor deposition (MOCVD) process similar to that employed by the electronics industry to manufacture advanced optoelectronic devices such as LEDs, diode lasers, and space solar cells. A particular challenge of this approach is the achievement of adequate quality thin-film CZT at a deposition temperature that will not degrade the TFT array. Our efforts to date have shown that although deposition can occur at temperatures as low as 250°C (the maximum allowable temperature for amorphous silicon TFTs), deposition rates are extremely slow and expensive, difficult-to-obtain precursors are required. Raising the temperature to 450°C helps solve these problems, but requires the use of high temperature TFTs such as polycrystalline silicon. Cadmium selenide (CdSe) TFTs may be another option, but their availability is extremely limited. Significant progress has been made in achieving the necessary thin-film CZT materials and device properties, but there still remain several challenges to be overcome that include high leakage current, slow deposition rate, and potentially high materials usage.

This work was supported by the U.S. Army Medical Research and Materiel Command under Contract DAMD17-96-C-6086.

4 CONCLUSIONS

At the end of this program Spire had proved that we developed a manufacturable process for deposition of thin films of (Cd, Zn)Te onto crystalline silicon TFT arrays that could be used for radiation detector readout. These substrates were not explored earlier during the research as all commercial suppliers of medical x-ray equipment who expressed interest in our possible new product explicitly wanted to use only amorphous silicon materials. If a product were to result from this research, Spire felt that we had to be responsive to the imperatives of potential customers.

Technically, the program failed to reach its goals due to a fundamental materials problem not well understood at this time. The (Cd, Zn)Te thin film material had low resistance compared to bulk grown ingots. Manufacturers are exploring use of bulk material for similar devices (NOVA R&D Inc., Riverside CA, paper E33 at ERA of HOPE conference in 2000). They will be more costly than thin film devices if the latter would have worked.

What could be wrong? I will compare results to other semiconductor materials. For crystal silicon, vapor deposited films have electrical resistance up to 10,000 ohm-cm compared to a best value of about 50,000 to 100,000 ohm-cm for bulk grown material. These very good results were pioneered by Spire Corporation, developed into a business for testing the purity of source gases, and sold. If CdZnTe would have a similar drop of only one order of magnitude, which was expected, the radiation detectors would have easily been feasible. We believe that low temperature crystal growth and low partial pressures of constituents, compared to bulk growth conditions, leads to creation of point defects that can intrinsically dope the films, increasing conductance. We have no formal proof for these possible conclusions.

5 REFERENCES

- 1 W. Zhao, I. Blevis, S. Germann, J.A. Rowlands, D. Waechter and Z. Huang, "Digital Radiology using Active Matrix Readout of Amorphous Selenium: Construction and Evaluation of a Prototype Real-time Detector," *Med. Phys.* **24**, 1834 (1997).
- 2 K. S. Shah, P. Bennett, Y. Dmitriev, L. Cirignano, M. Klugerman, M.R. Squillante, R.A. Street, J.T. Rahn and S.E. Ready, "PbI₂ for High Resolution Digital X-ray Imaging," *SPIE Proc.* **3770**, 164 (1999).
- 3 M. Schieber, H. Hermon, A. Zuck, A. Vilensky, L. Melekhov, R. Shatunovsky, E. Meerson and H. Saado, "Polycrystalline Mercuric Iodide Detectors," *SPIE Proc.* **3770**, 146 (1999).
- 4 D.R. Ouimette, R.M. Iodice, P-J Kung and L. Lynds, "A Real-time X-ray Image Sensor Using a Thallium Bromide Photoconductor," *SPIE Proc.* **3770**, 156 (1999).
- 5 JA Rowlands, SO Kasap, "Amorphous photoconductors usher-in digital x-ray imaging", Physics Today (November, 1997)
6. JA Rowlands, J Yorkston, "Flat panel detectors for digital radiology," pp. 223-328 In: *Medical Imaging Volume 1. Physics and Psychophysics* Edited by: J Beutel, HL Kundel and RL Van Metter (SPIE, Bellingham, 2000)
7. KS Shah, P Bennett, M Klugerman, LP Moy, G Entine, D Ouimette, R Aikens, "Lead Iodide Films for X-ray Imaging", Proc. SPIE **3032**, 395 (1997)
8. A Niemelä, H Sipilä, "Evaluation of CdZnTe detectors for soft x-ray applications", IEEE Trans. Nucl. Sci. **41**, 1054 (1994)

9. Z Huang, G DeCrescenzo, JA Rowlands, "Signal and noise analysis using a transmission line model for large area flat-panel x-ray imaging sensors", *Proc. SPIE* **3659** 76-89 (1999)
10. HB Barber, HH Barrett, FL Augustine, "Development of a 64x64 CdZnTe array and associated readout integrated circuit for use in nuclear medicine", *Journal of Electronic Materials*, **26**, 765 (1997)
11. R Sudharsanan, T Parodos, A Ruzin, Y Nemirovsky, NH Karam "CdZnTe photodiode arrays for medical imaging", *Journal of Electronic Materials*, **25**, 1318 (1996)
12. J D Eskin, HH Barrett, HB Barber, J M Woolfenden "The effect of pixel geometry on spatial and spectral resolution in CdZnTe imaging array", (To be published)
13. JD Eskin, HB Barber, HH Barrett "Variations in pulse-height spectrum and pulse timing in CdZnTe pixel array detectors", *SPIE* **2859**, 46 (1996)
14. R Fahrig, JA Rowlands, MJ Yaffe, "X-ray imaging using amorphous selenium: Detective quantum efficiency of photoconductive image receptors for digital mammography", *Med. Phys.* **22**, 153-160 (1995)
15. R Fahrig, JA Rowlands, MJ Yaffe, "X-ray imaging using amorphous selenium: Optimal spectra for digital mammography", *Med. Phys.* **23** 557-567 (1996)
16. DC Hunt, W Zhao, JA Rowlands, "Detective quantum efficiency of direct, flat panel detectors for fluoroscopy", *Proc. SPIE* **3336**, 195-201 (1998)
17. R. Korenstein, W.E. Hoke, P.J. Lemonias, K.T. Higa, and D.C. Harris, "Metalorganic growth of HgTe and CdTe at low temperature using diallyltelluride", *J. Appl. Phys.* **62**, 4929 (1987).
18. W.E. Hoke and P.J. Lemonias, "Low-temperature metalorganic growth of CdTe and HgTe films using ditertiarybutyltelluride", *Appl. Phys. Lett.* **48**, 1669 (1986).
19. D. Shenai-Khatkhate, "Tellurium and Selenium Source Review", Morton International Technical Bulletin #9/90 (1990).
20. MJ Yaffe, JA Rowlands, "X-ray detectors for digital radiology", *Physics in Medicine and Biology* **42**, 1-39 (1997)
21. RE Johanson, SO Kasap, JA Rowlands, B Polischuk, "Metallic electrical contacts to stabilized amorphous selenium for use in x-ray image detectors", *J. Non-Cryst. Solids*, **227-230** 1359-1362 (1998)
22. W Zhao, WG Ji, JA Rowlands, A Debrie, "Investigation of imaging performance of amorphous selenium flat-panel detectors for digital mammography", *Proc. SPIE* (2001)
23. IM Blevis, DC Hunt, JA Rowlands, "X-ray imaging using amorphous selenium: Determination of Swank factor by pulse height spectroscopy", *Med. Phys.*, **25**, 638-641 (1998)
24. RW Swank, "Absorption and noise in x-ray phosphors", *J. Appl. Phys.* **44** 4199-4203 (1973)
25. M Drangova, JA Rowlands, "Optical factors affecting the detective quantum efficiency of radiographic screens", *Med. Phys.* **13**, 150-157 (1986)
26. DP Trauernicht, R Van Metter, "The measurement of conversion noise in x-ray intensifying screens", *Proc. SPIE* **914** 100-116 (1988)
27. A Ginzburg, CE Dick, "Image information transfer properties of x-ray intensifying screens in the energy range from 17 to 320 keV", *Med. Phys.* **20** 1013-1021 (1993)

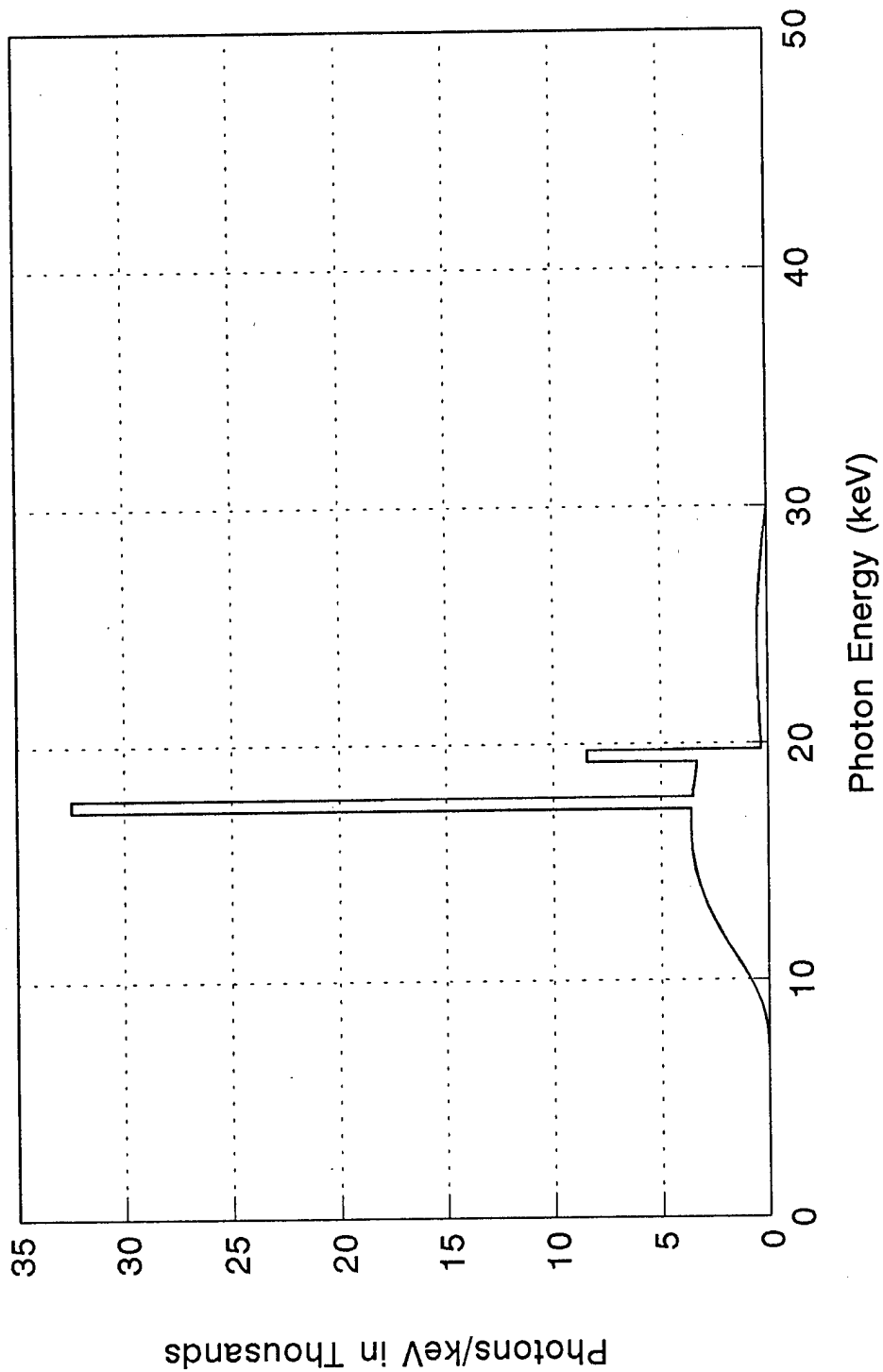
- 28. JA Rowlands, KW Taylor, "Absorption and noise in cesium iodide x-ray image intensifiers", *Med. Phys.* **10** 786-795 (1983)
- 29. R Fahrig, JA Rowlands, MJ Yaffe, "X-ray imaging using amorphous selenium: Detective quantum efficiency of photoconductive image receptors for digital mammography", *Med. Phys.* **22**, 153-160 (1995)
- 30. IM Blevis, DM Hunt, JA Rowlands, "X-ray imaging using amorphous selenium: Determination of Swank factor by pulse height spectroscopy", *Med. Phys.* **25** 638-641 (1998)
- 31. KL Yip, BR Whiting, TE Kocher, DP Trauernicht, RL Van Metter, "Understanding the relative sensitivity of radiographic screens to scattered radiation," *Med. Phys.* **23** 1727-1737 (1996)
- 32. W Zhao, IM Blevis, DF Waechter, Z Huang, JA Rowlands, "Digital radiology using active matrix readout of amorphous selenium: Construction and evaluation of a prototype real-time detector", *Med. Phys.*, **24**, 1834-1843 (1997)
- 33. R. Birch and M. Marshall, "Catalogue of Spectral Data for Diagnostic X-rays," Hospital Physicists Association (1979).
- 34. Oettinger, K., Hofmann, D.M., Efros, A.L., Meyer, B.K., Salk, M. and Benz, K.W., *J. Appl. Phys.* **71**, 4523 (1992).
- 35. E. Storm and I. Israel, "Photon Cross Sections from 0.001 to 100 MeV for Elements 1 through 100," Los Alamos Scientific Laboratory Report LA-3753 (1967).

Spire Corporation		
Contract No. DAMD17-96-C-6086		
List of Personnel on this Research Effort		
Amero, Michelle K.		
Bennett, Paul R.		
Breen, Wilson F.		
Cooke, Pauline M.		
Cunha, Robert M.		
Drake, Brian J.		
Gagnon, Edward D.		
George, Douglas J.		
Greenwald, Anton C.		
Halverson, Ward D.		
Haven Jr., Victor E.		
Kalkhoran, Nader M.		
Mak, Paul S.		
Mao, Wendy L.		
Marchant, Scott A.		
Markham, David P.		
Mastrovito, Andre		
McNulty, Daniel D.		
Muldoon, Cynthia M.		
Neal, William R.		
Nollet, Curt E.		
Paradiso, David A.		
Reader, Connie R.		
Reiche, Christopher G.		
Ryan, Timothy J.		
Santosuoso, Matthew		
Serreze, Harvey B.		
Sudharsanan, Rengarajan		
Sullivan, Susan B.		
Ta, Tri M.		
Taylor, Daniel R.		
Toney, James E.		
Trivedi, Dhrupad A.		
Trivedi, Deborah Lehr		
Turvey, Anthony E.		
Vakerlis, George D.		
Vernon, Stanley M.		

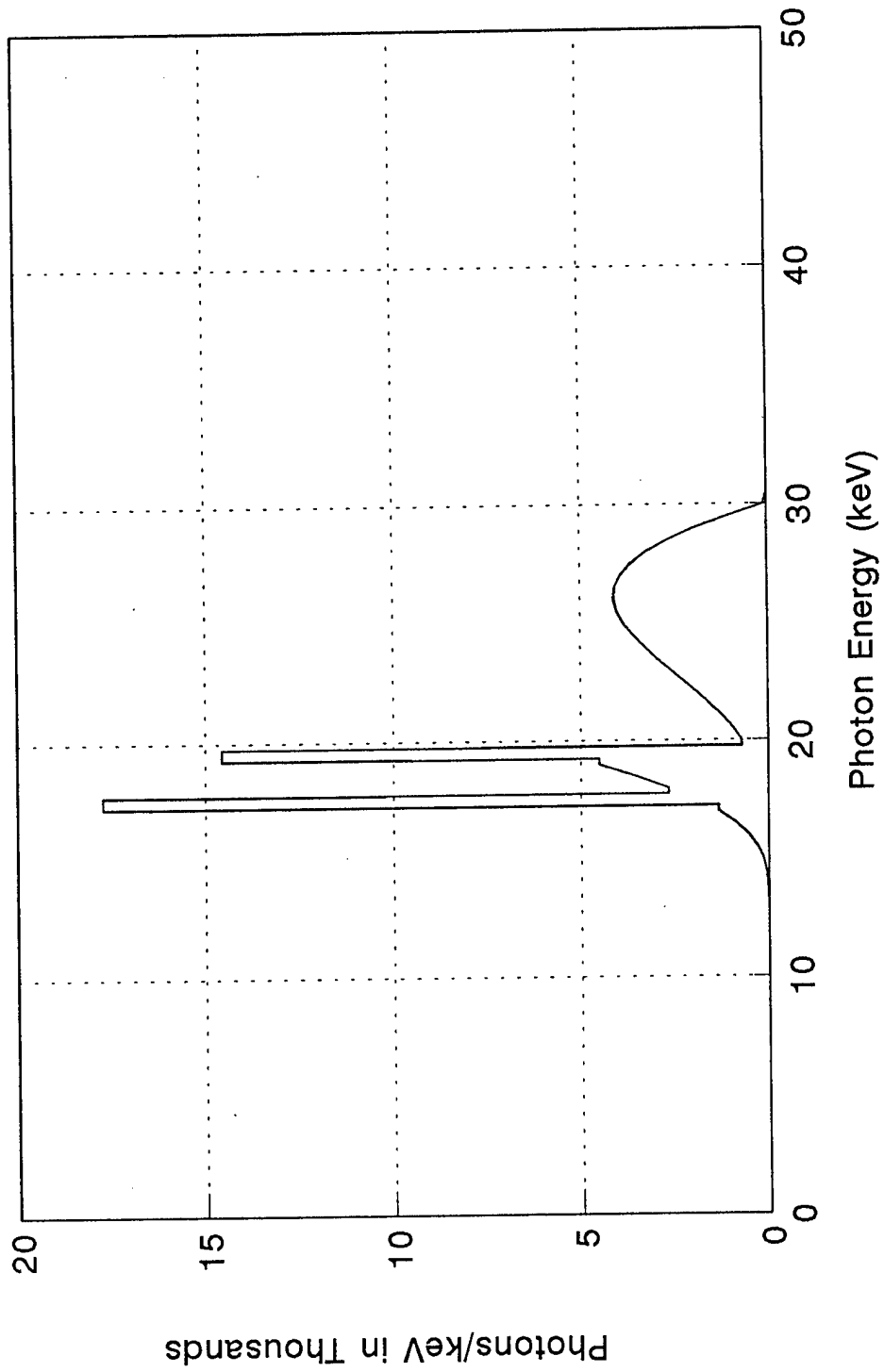
APPENDIX A

Calculation of Energy Absorption Efficiency for Several X-ray Sources and Absorber Materials

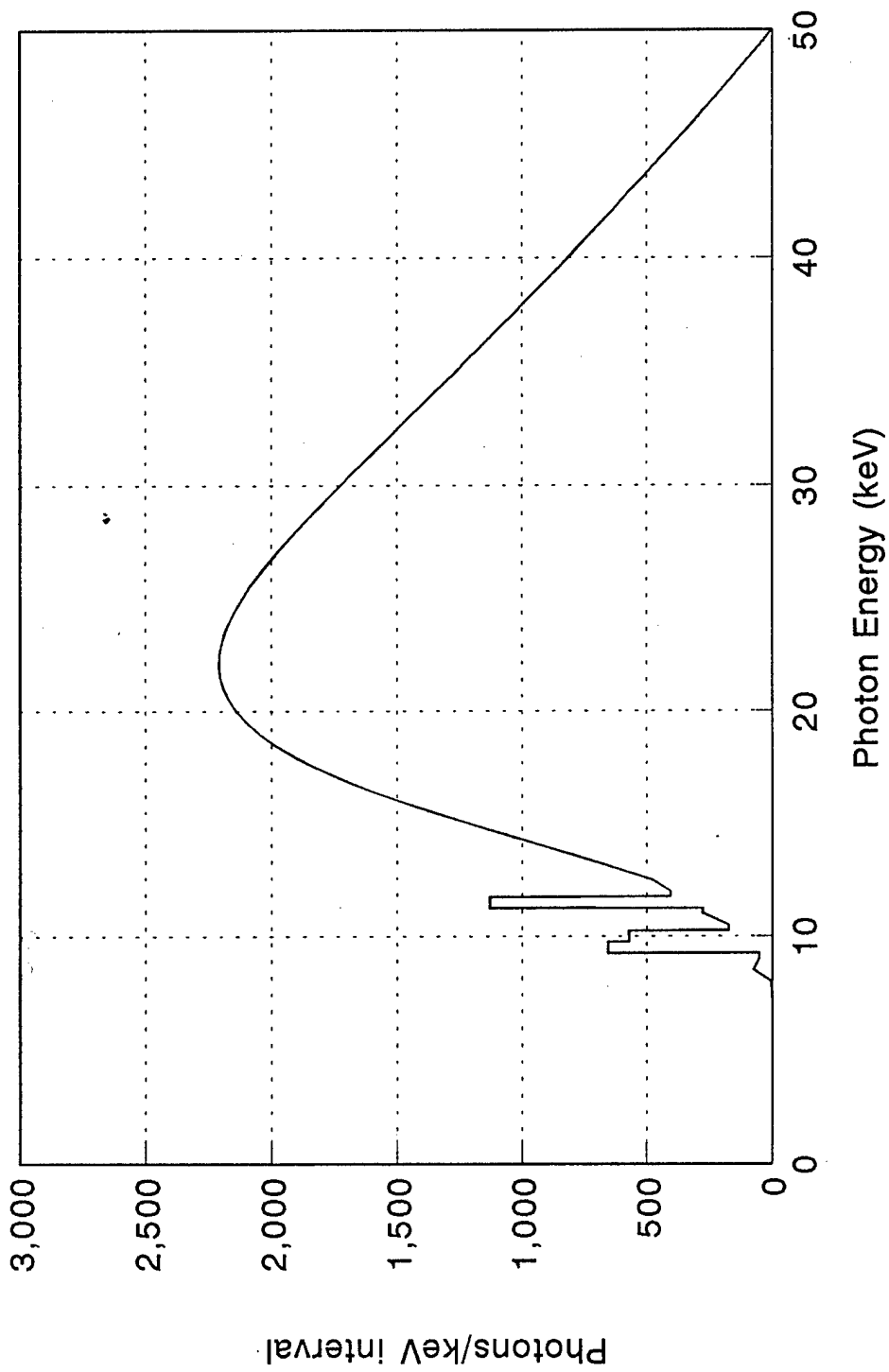
30 kV CONSTANT POTENTIAL X-RAY SPECTRUM
Molybdenum Target 1.0 mm Be 0.03 mm Mo



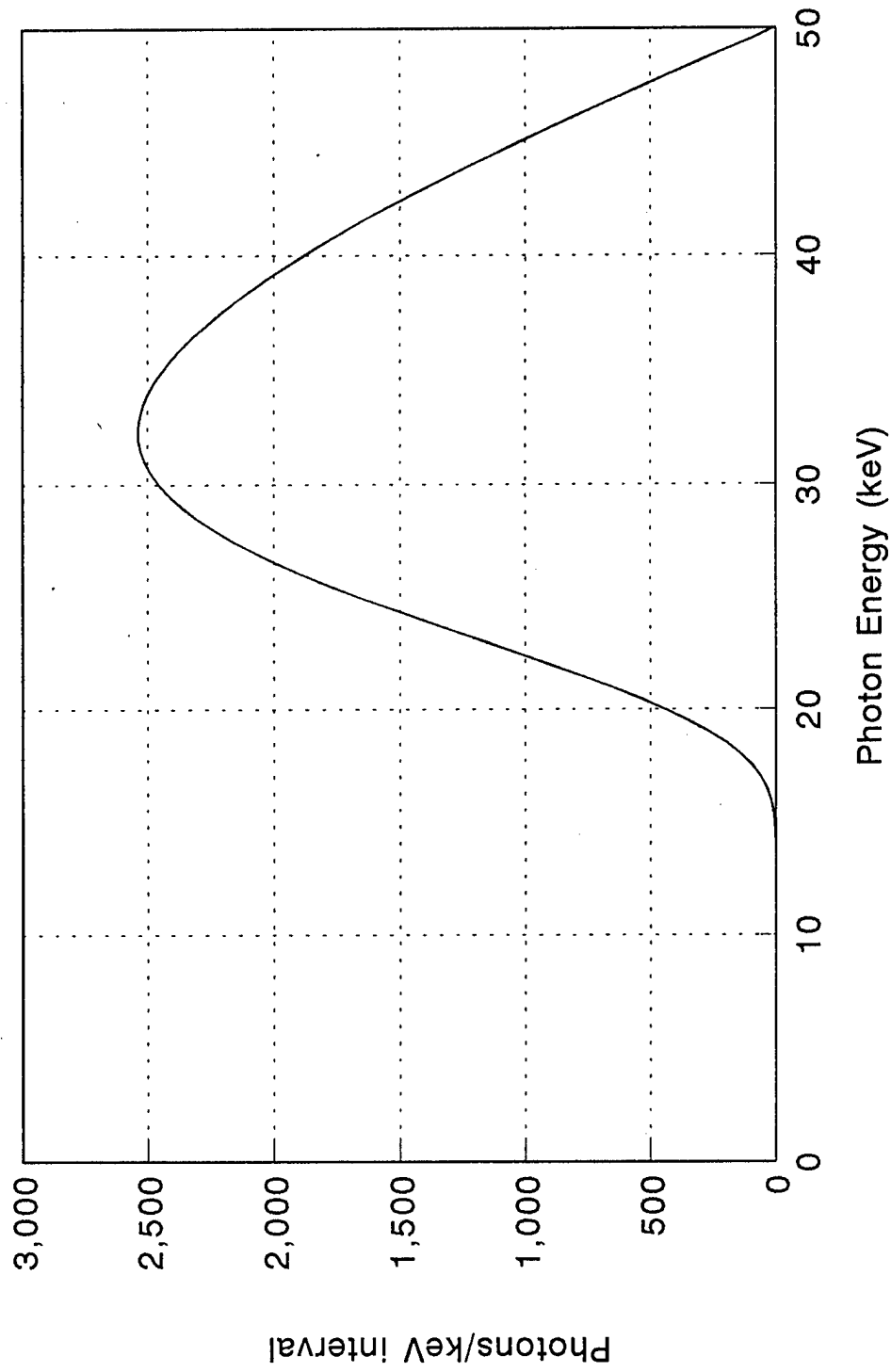
30 kV CONSTANT POTENTIAL X-RAY SPECTRUM
Molybdenum Target 1.0 mm Be 0.03 mm Mo 5.0 cm Tissue



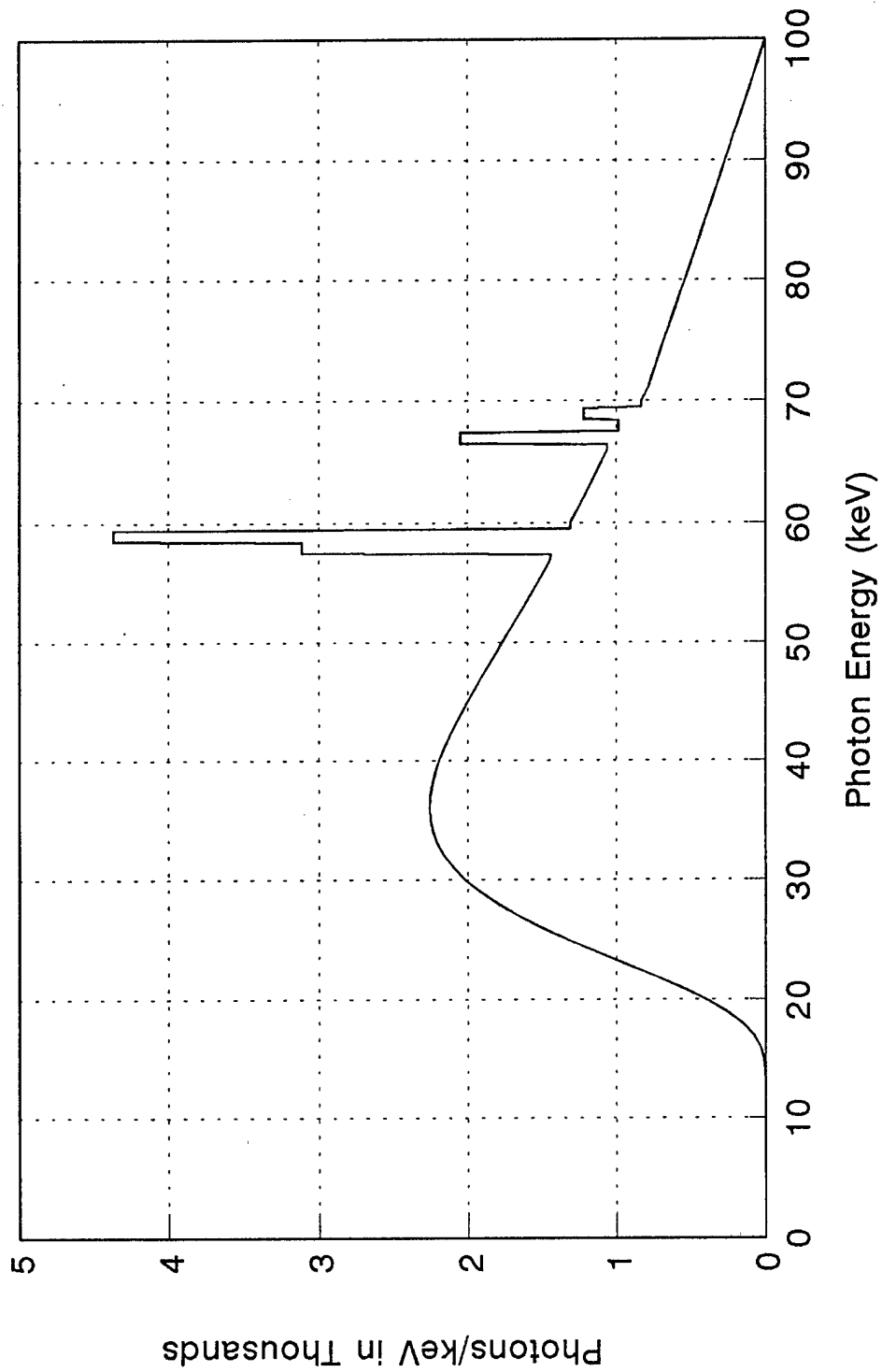
50 KV CONSTANT POTENTIAL X-RAY SPECTRUM
Tungsten Target 1.0 mm Be 0.5 mm Al



50 kV CONSTANT POTENTIAL X-RAY SPECTRUM
Tungsten Target 1.0 mm Be 0.5 mm Al 5 cm Tissue

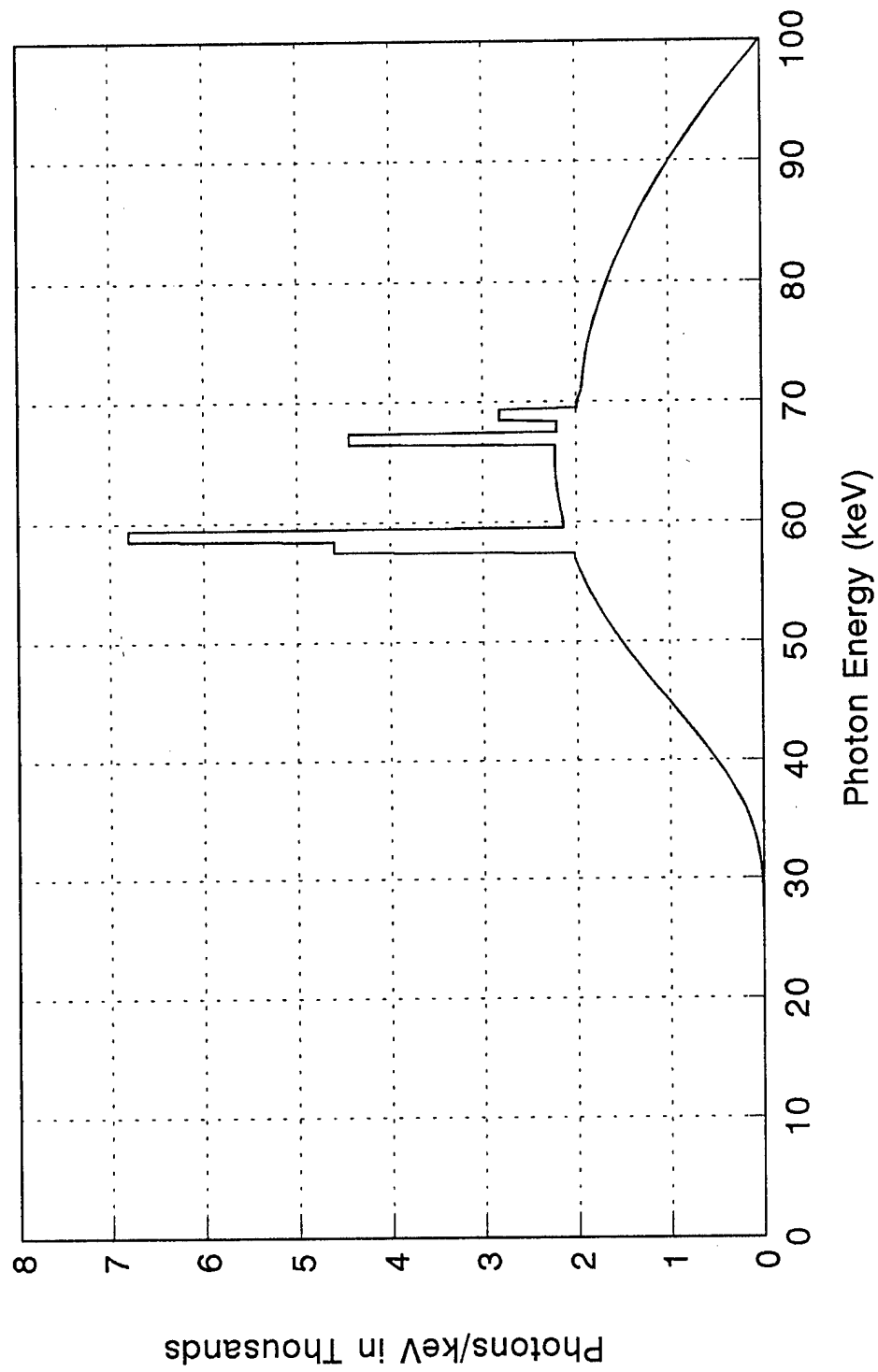


100 kV CONSTANT POTENTIAL X-RAY SPECTRUM
Tungsten Target 2.5 mm Al

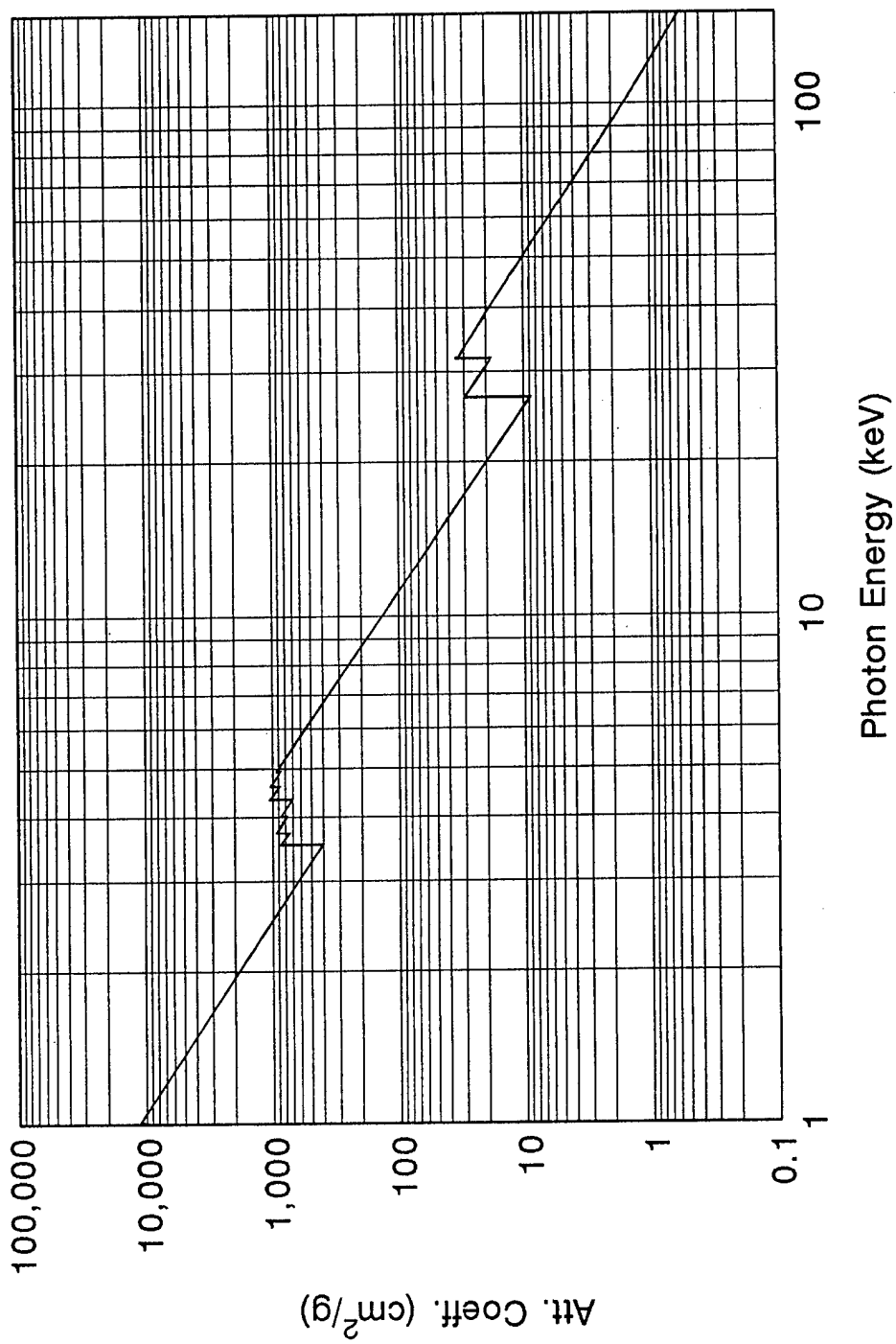


100 kV CONSTANT POTENTIAL X-RAY SPECTRUM

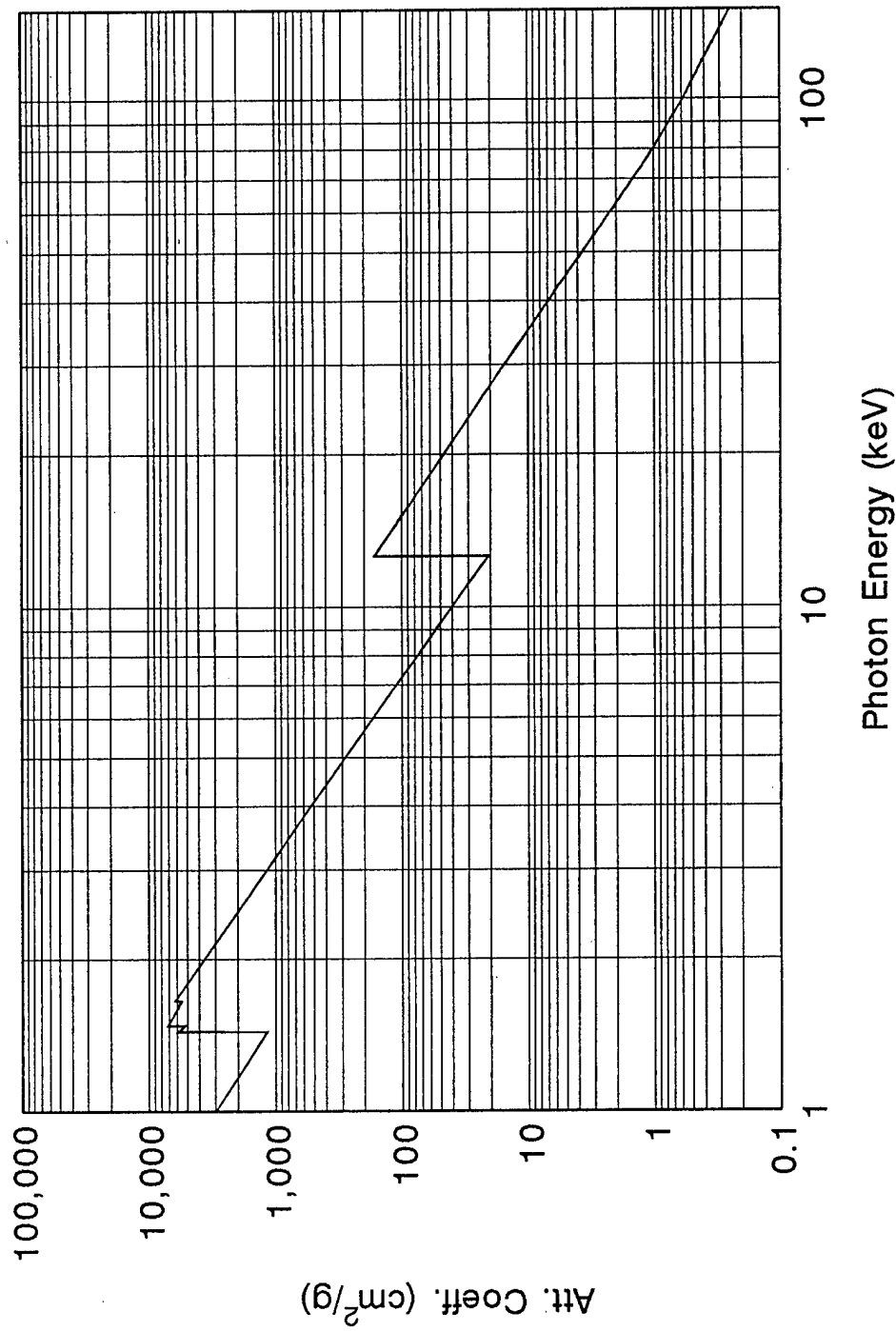
Tungsten Target 2.5 mm Al 18.5 cm Tissue + 1.5 cm Bone



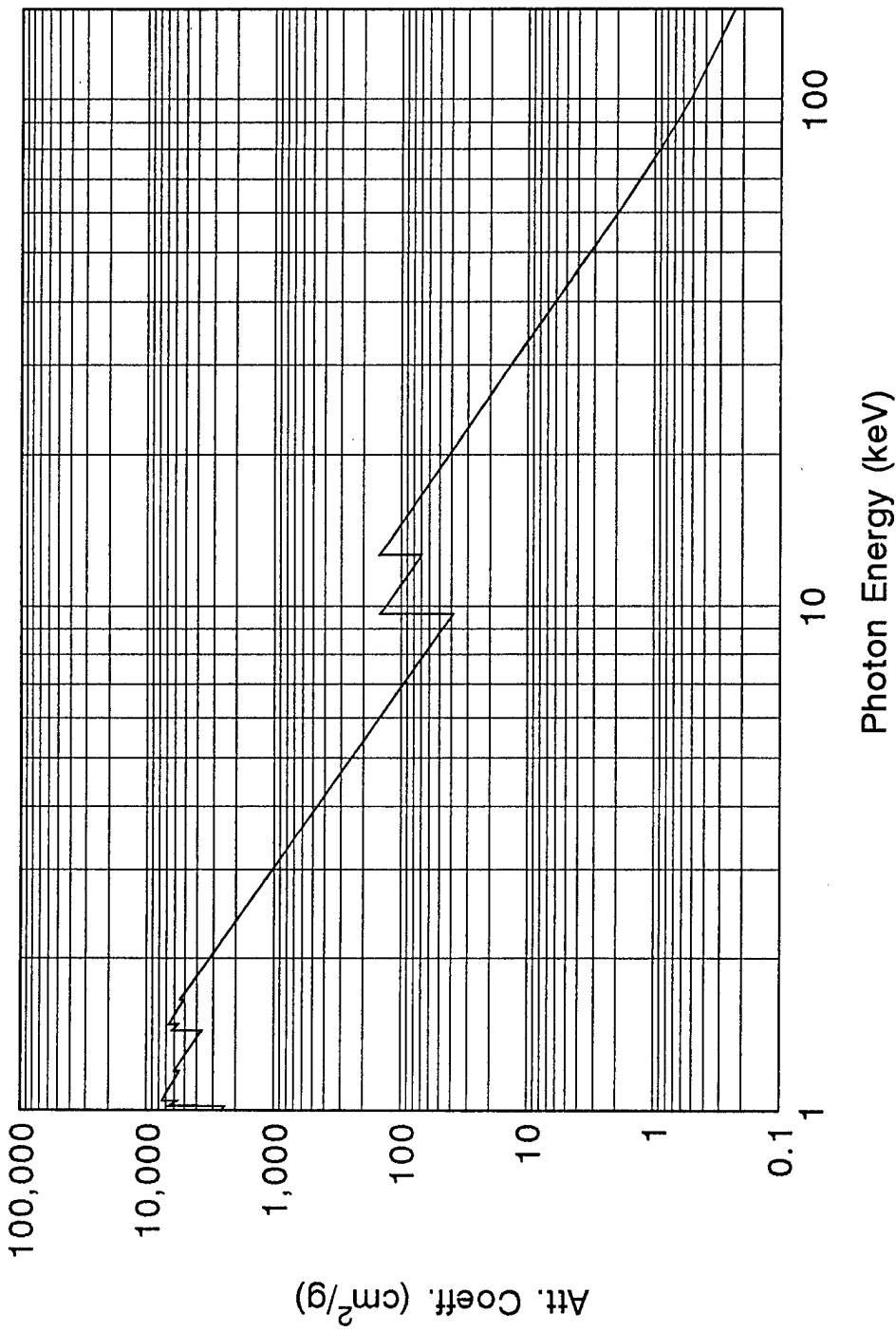
X-RAY ATTENUATION COEFFICIENTS
CdTe and CdZnTe Storm and Israel LA-3753 (1967)



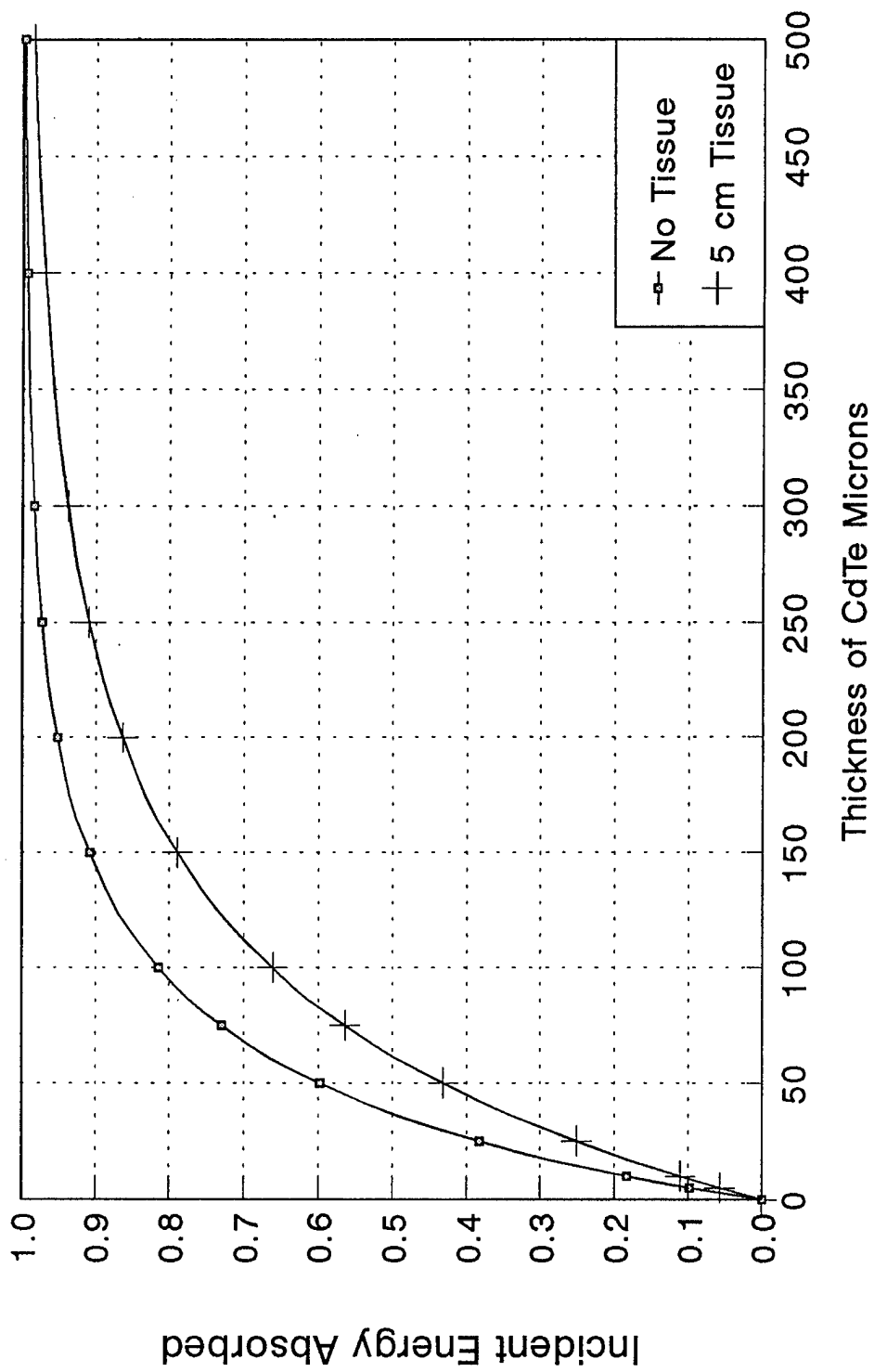
X-RAY ATTENUATION COEFFICIENTS
Selenium Storm and Israel LA-3753 (1967)



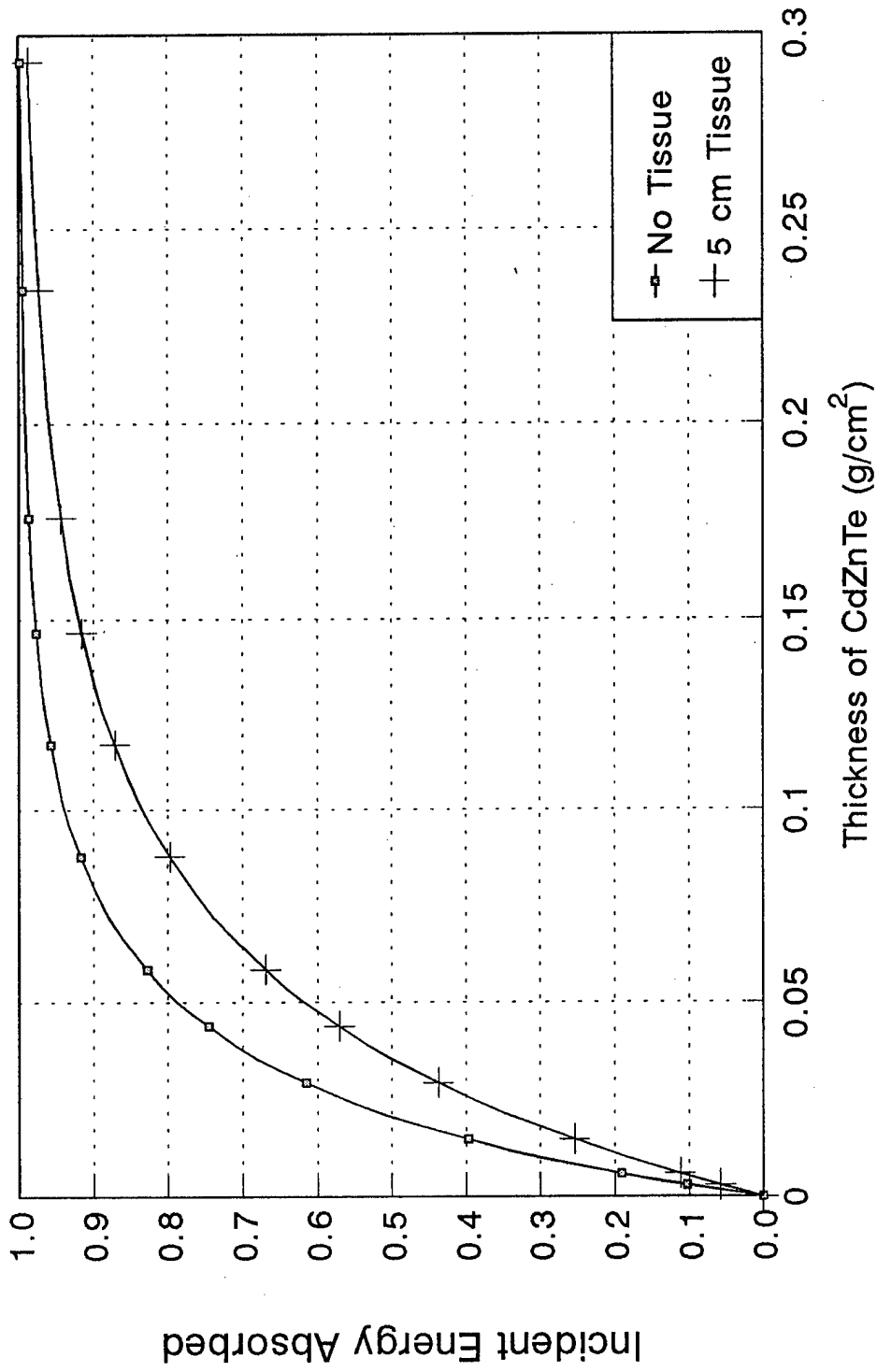
X-RAY ATTENUATION COEFFICIENTS
ZeSe Storm and Israel LA-3753 (1967)



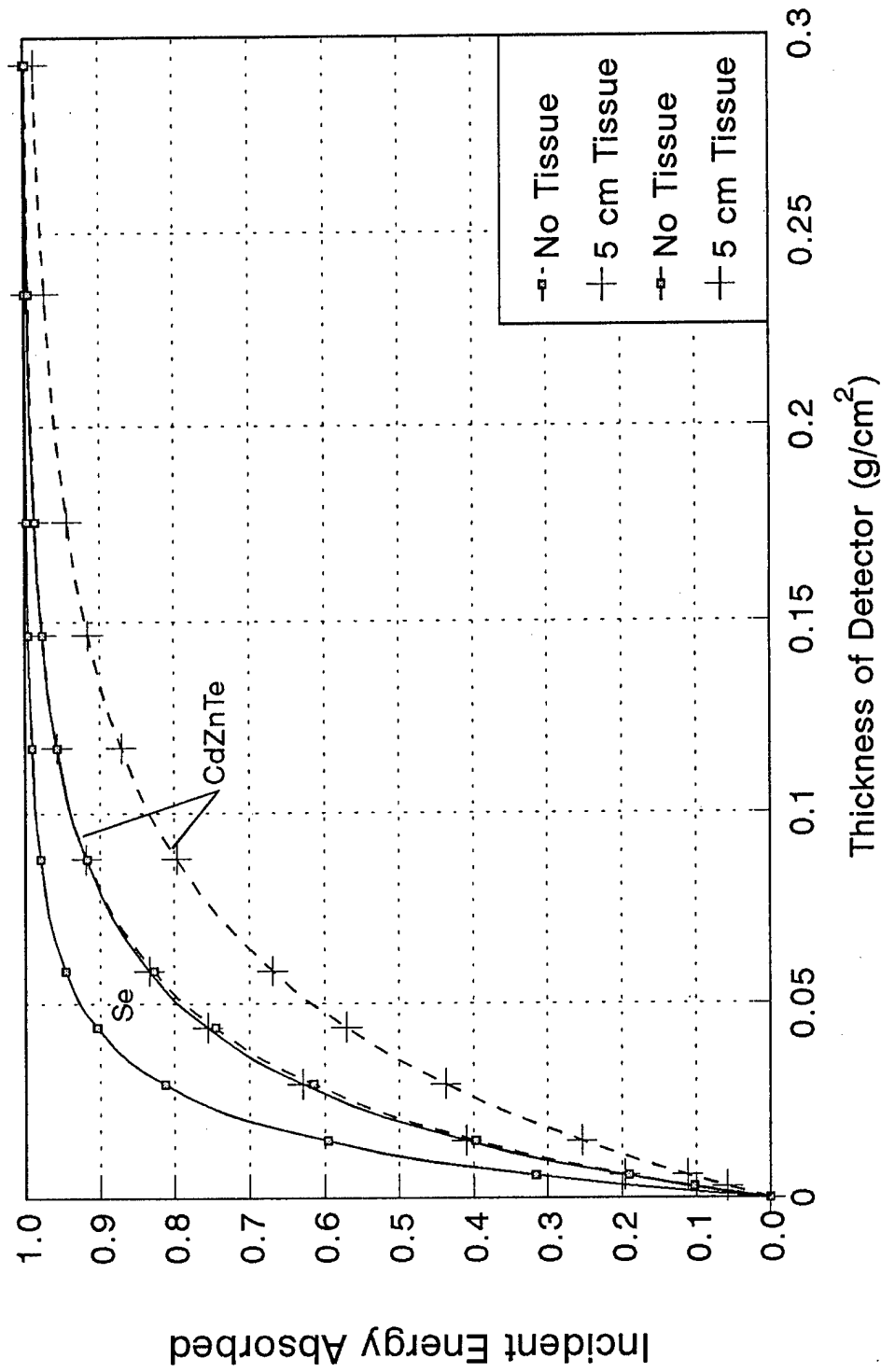
ENERGY DEPOSITION IN CdTe AS A FUNCTION OF THICKNESS
30 kV Molybdenum Spectrum 1.0 mm Be 0.03 mm Mo



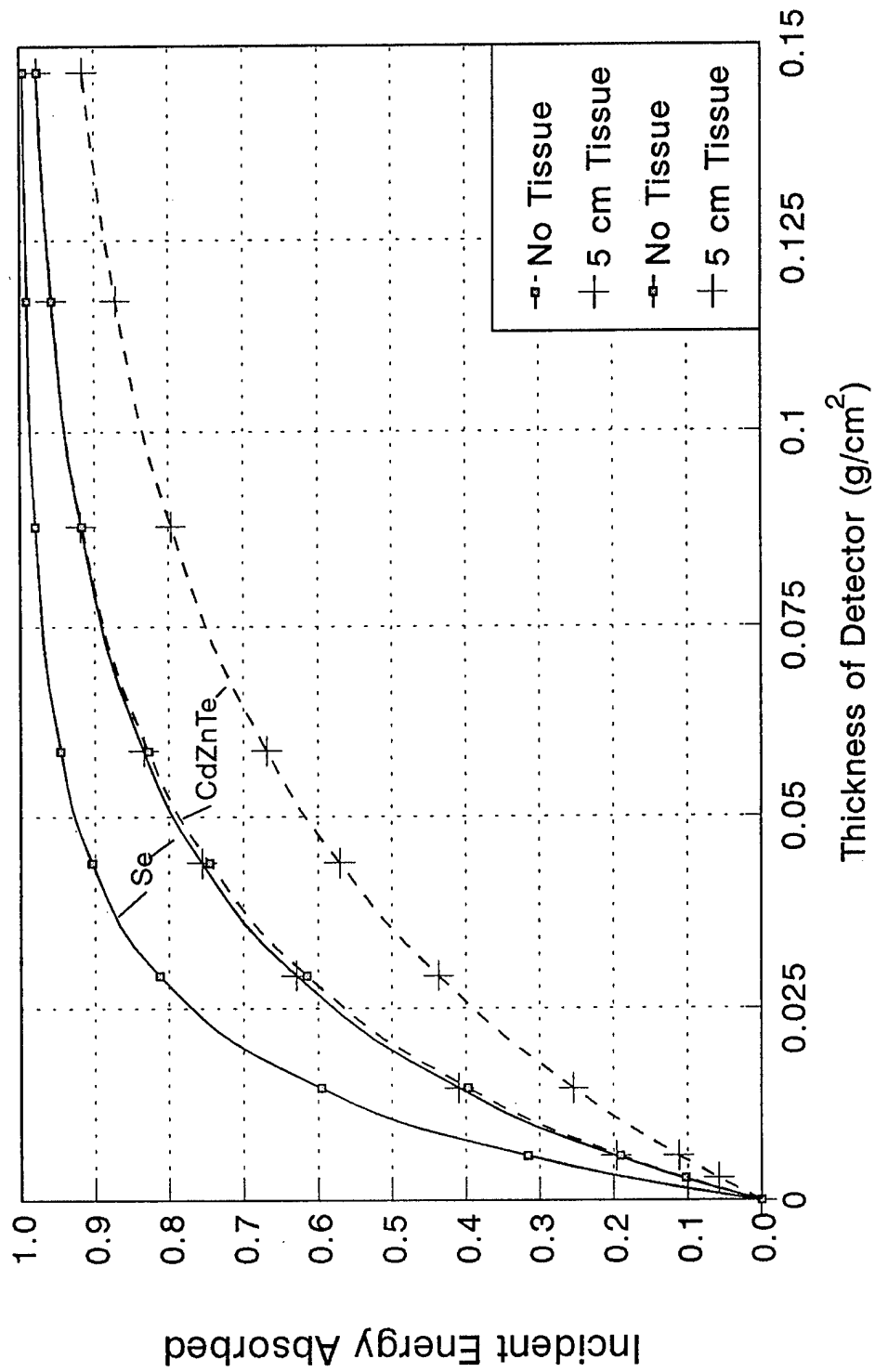
ENERGY DEPOSITION IN CdZnTe AS A FUNCTION OF THICKNESS
30 kV Molybdenum Spectrum 1.0 mm Be 0.03 mm Mo



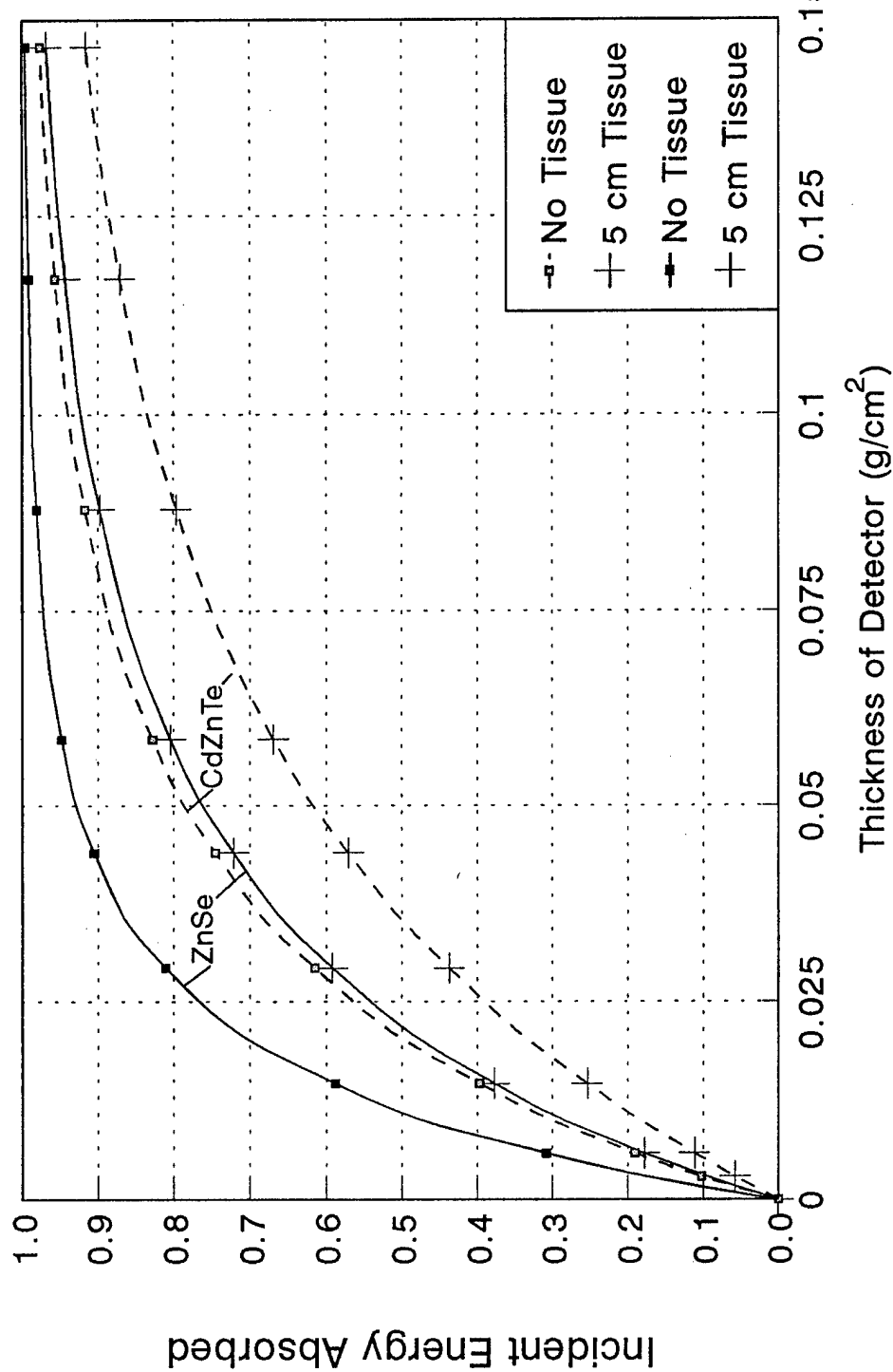
ENERGY DEPOSITION IN CdZnTe AND Se AS A FUNCTION OF THICKNESS
30 kV Molybdenum Spectrum 1.0 mm Be 0.03 mm Mo



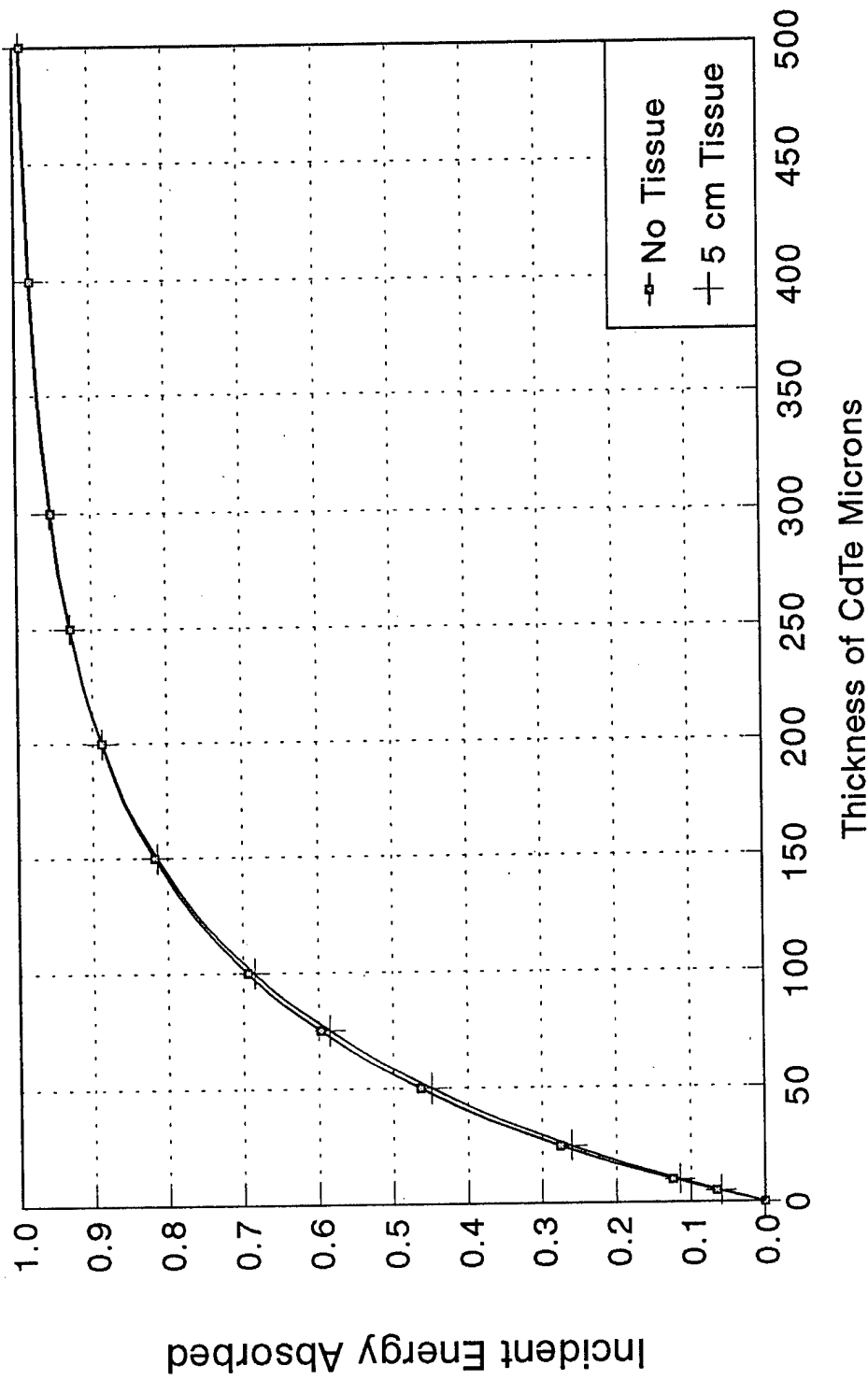
ENERGY DEPOSITION IN CdZnTe AND Se AS A FUNCTION OF THICKNESS
30 kV Molybdenum Spectrum 1.0 mm Be 0.03 mm Mo



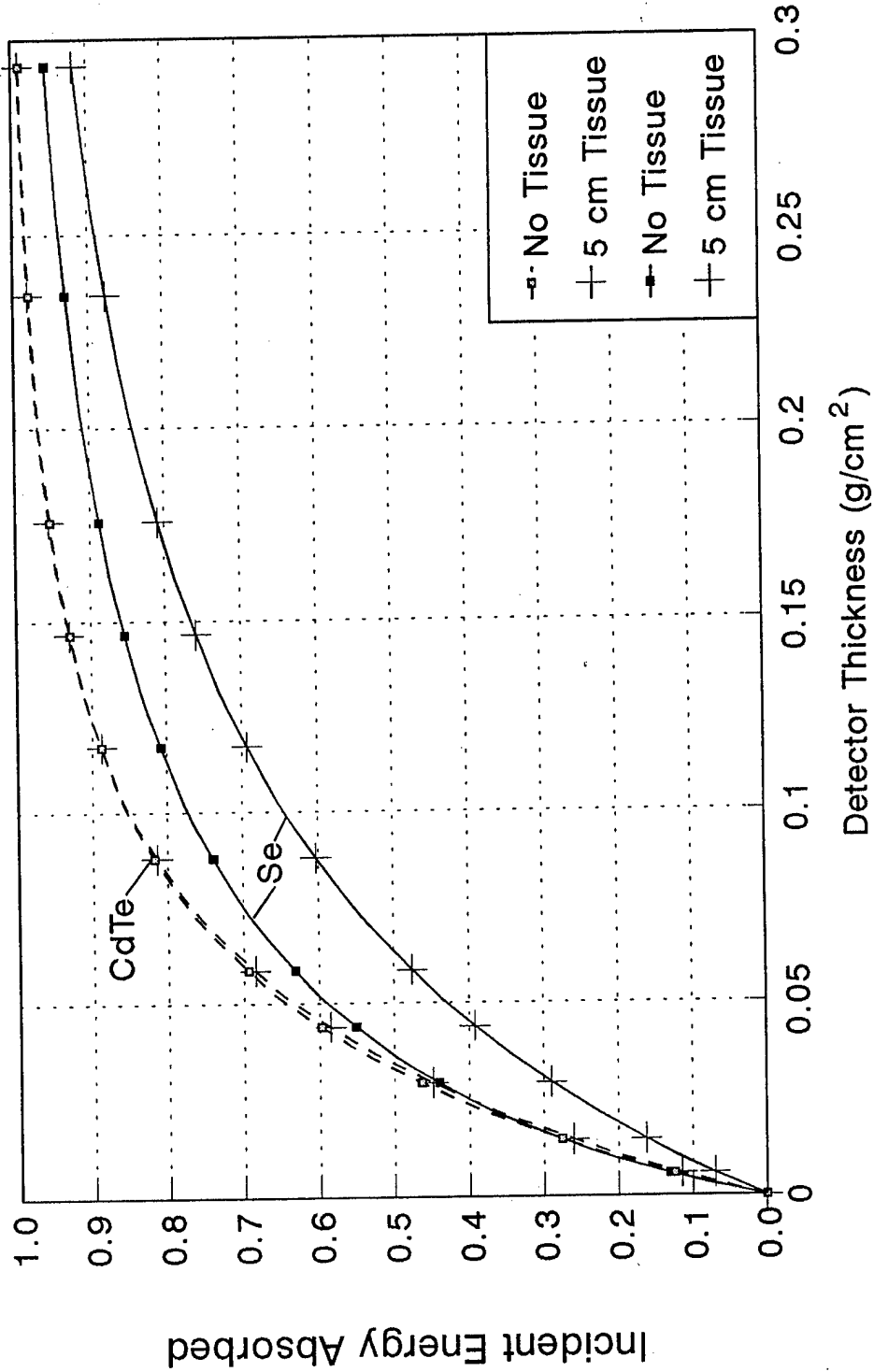
ENERGY DEPOSITION IN CdZnTe AND ZnSe AS A FUNCTION OF THICKNESS
30 kV Molybdenum Spectrum 1.0 mm Be 0.03 mm Mo



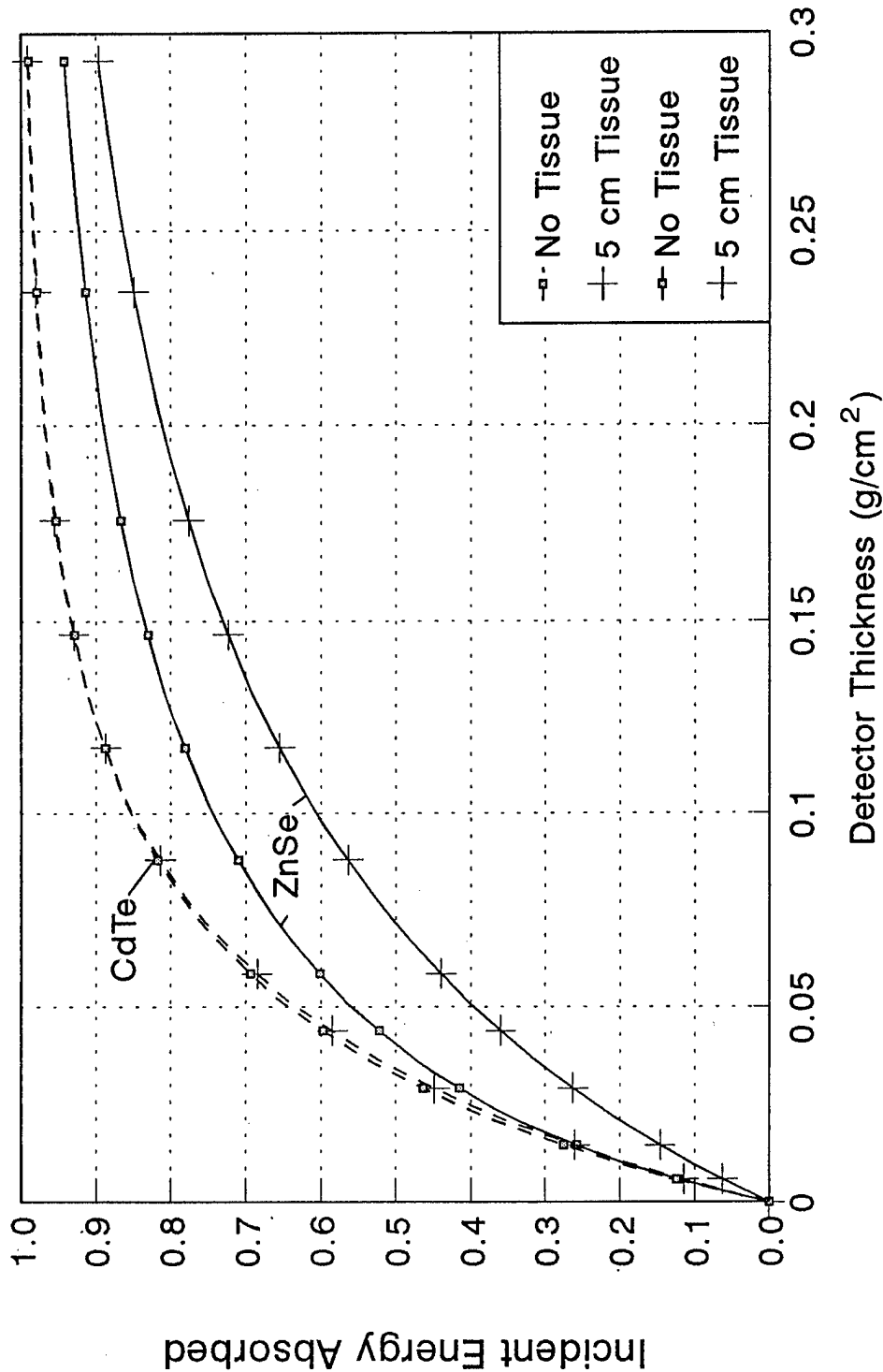
ENERGY DEPOSITION IN CdTe AS A FUNCTION OF THICKNESS
50 KV Tungsten Spectrum 1.0 mm Be 0.5 mm Al



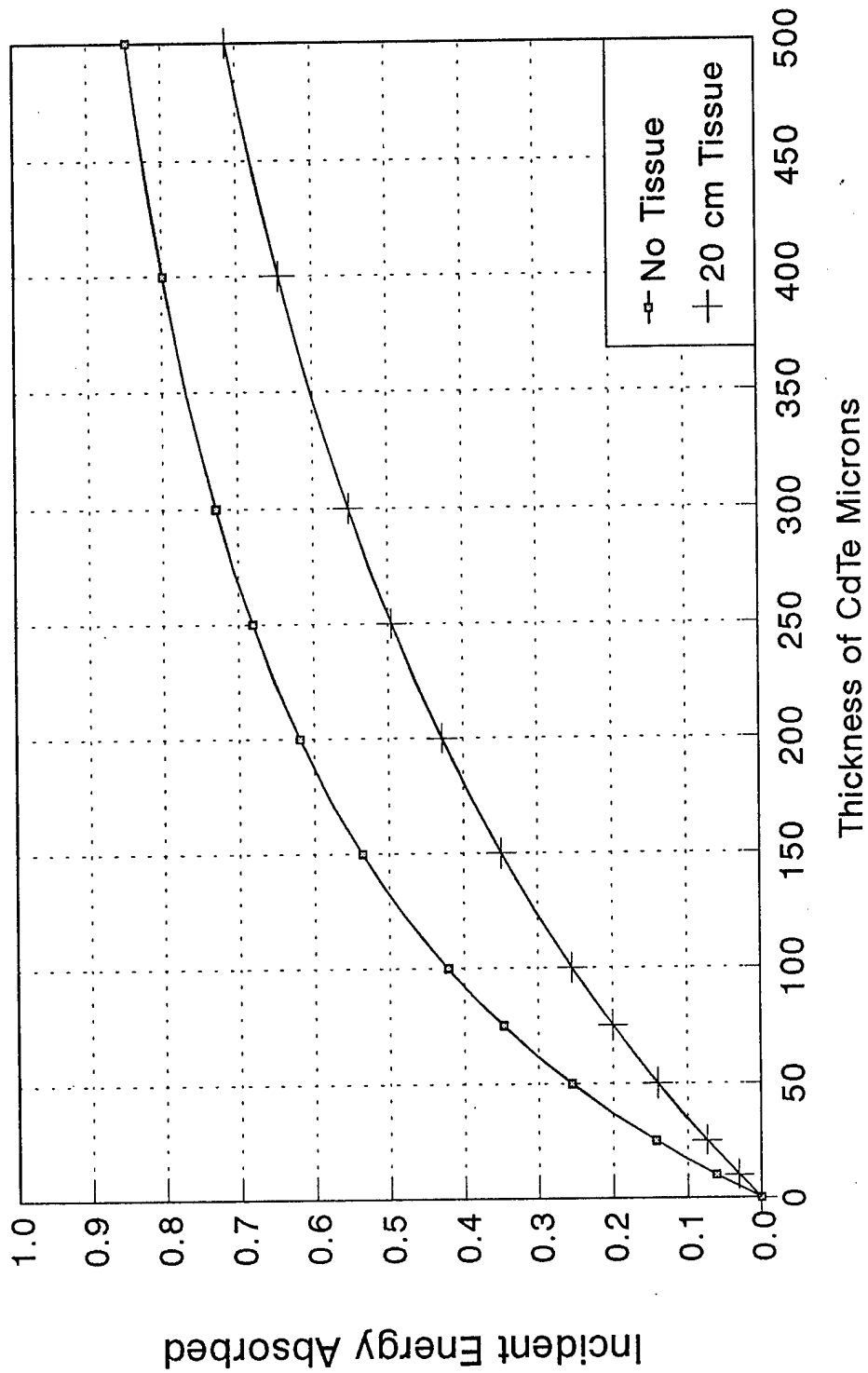
ENERGY DEPOSITION IN CdTe AND Se AS A FUNCTION OF THICKNESS
50 kV Tungsten Spectrum 1.0 mm Be 0.5 mm Al



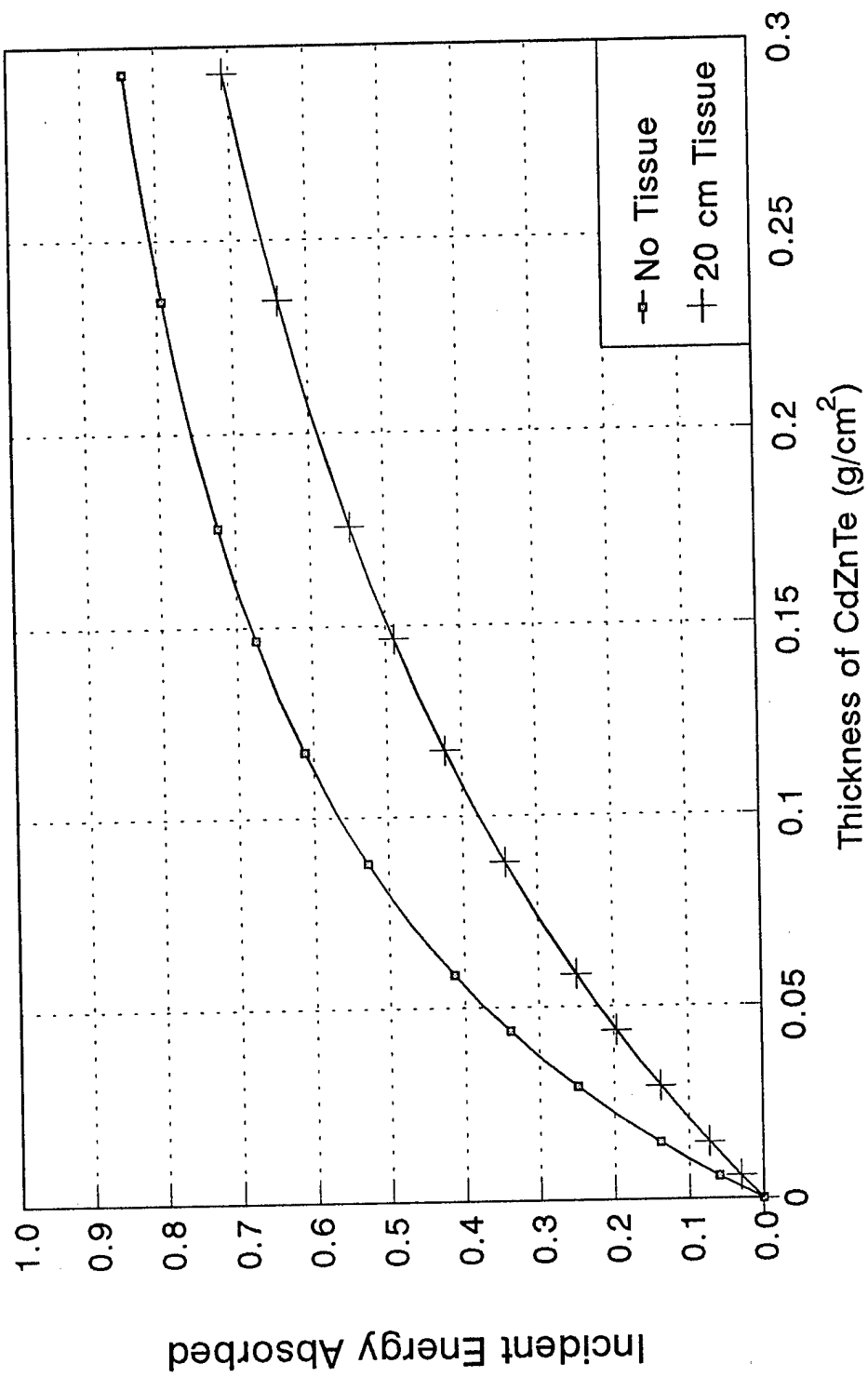
ENERGY DEPOSITION IN CdTe AND ZnSe AS A FUNCTION OF THICKNESS
50 kV Tungsten Spectrum 1.0 mm Be 0.5 mm Al



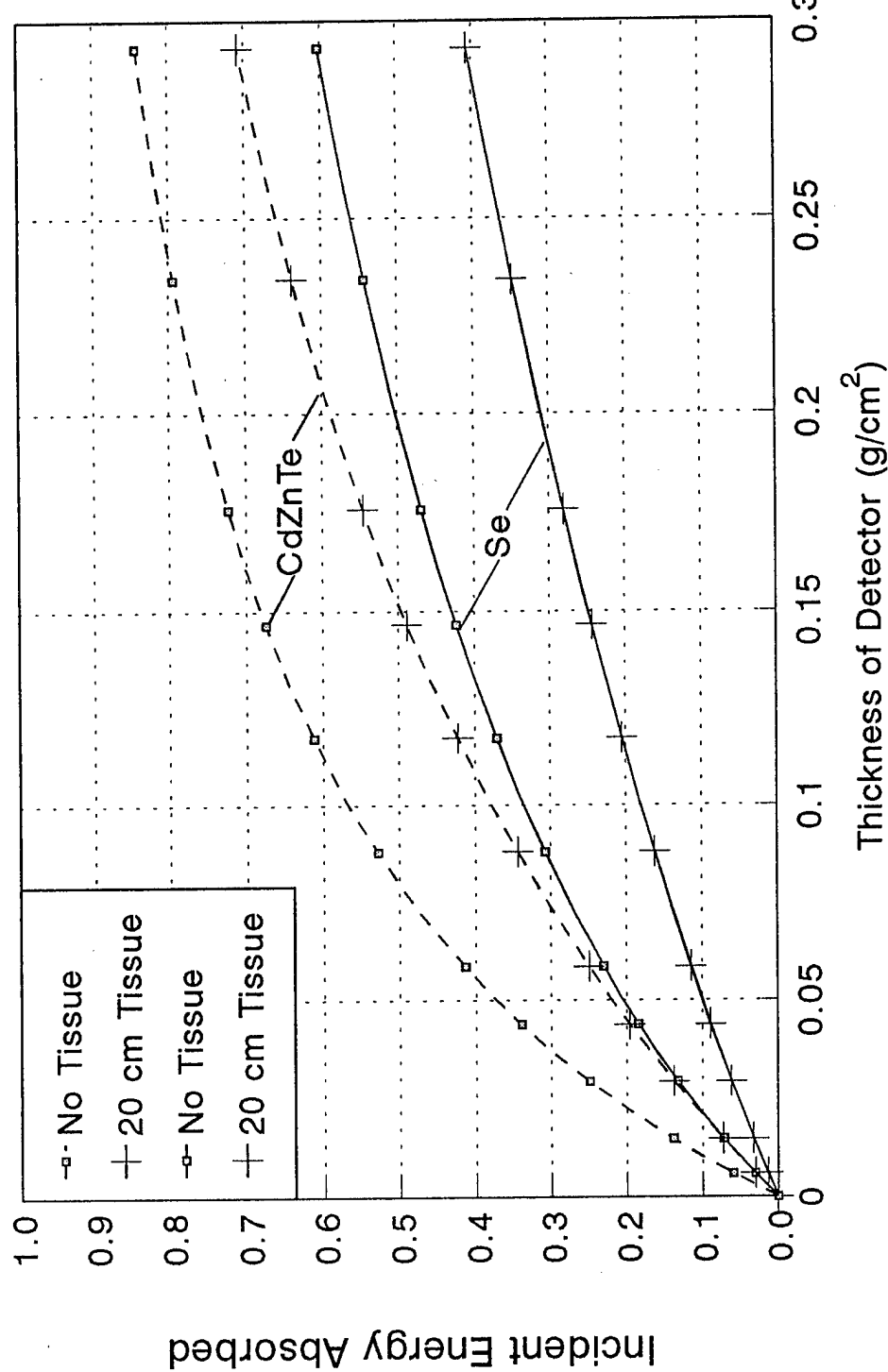
ENERGY DEPOSITION IN CdTe AS A FUNCTION OF THICKNESS
100 kV Tungsten Spectrum 2.5 mm Al



ENERGY DEPOSITION IN CdZnTe AS A FUNCTION OF THICKNESS
100 kV Tungsten Spectrum 2.5 mm Al



ENERGY DEPOSITION IN CdZnTe AND Se AS A FUNCTION OF THICKNESS
100 kV Tungsten Spectrum 2.5 mm Al



ENERGY DEPOSITION IN CdZnTe AND Se AS A FUNCTION OF THICKNESS
100 kV Tungsten Spectrum 2.5 mm Al

